Springer

Dear Author,

Here are the proofs of your article.

- You can submit your corrections **online**, via **e-mail** or by **fax**.
- For **online** submission please insert your corrections in the online correction form. Always indicate the line number to which the correction refers.
- You can also insert your corrections in the proof PDF and **email** the annotated PDF.
- For fax submission, please ensure that your corrections are clearly legible. Use a fine black pen and write the correction in the margin, not too close to the edge of the page.
- Remember to note the **journal title**, **article number**, and **your name** when sending your response via e-mail or fax.
- **Check** the metadata sheet to make sure that the header information, especially author names and the corresponding affiliations are correctly shown.
- **Check** the questions that may have arisen during copy editing and insert your answers/ corrections.
- **Check** that the text is complete and that all figures, tables and their legends are included. Also check the accuracy of special characters, equations, and electronic supplementary material if applicable. If necessary refer to the *Edited manuscript*.
- The publication of inaccurate data such as dosages and units can have serious consequences. Please take particular care that all such details are correct.
- Please **do not** make changes that involve only matters of style. We have generally introduced forms that follow the journal's style.
  Substantial changes in content, e.g., new results, corrected values, title and authorship are not allowed without the approval of the responsible editor. In such a case, please contact the Editorial Office and return his/her consent together with the proof.
- If we do not receive your corrections **within 48 hours**, we will send you a reminder.
- Your article will be published **Online First** approximately one week after receipt of your corrected proofs. This is the **official first publication** citable with the DOI. **Further changes are, therefore, not possible.**
- The **printed version** will follow in a forthcoming issue.

Please note

After online publication, subscribers (personal/institutional) to this journal will have access to the complete article via the DOI using the URL: http://dx.doi.org/[DOI].
If you would like to know when your article has been published online, take advantage of our free alert service. For registration and further information go to: http://www.link.springer.com.

Due to the electronic nature of the procedure, the manuscript and the original figures will only be returned to you on special request. When you return your corrections, please inform us if you would like to have these documents returned.

Metadata of the article that will be visualized in OnlineFirst

ArticleTitle	Structure of Turbulence in Katabatic Flows Below and Above the Wind-Speed Maximum	
Article Sub-Title		
Article CopyRight	Springer Science+Business Media Dordrecht (This will be the copyright line in the final PDF)	
Journal Name	Boundary-Layer Meteorology	
Corresponding Author	Family Name	**Grachev**
	Particle	
	Given Name	**Andrey A.**
	Suffix	
	Division	NOAA Earth System Research Laboratory/Cooperative Institute for Research in Environmental Sciences
	Organization	University of Colorado
	Address	325 Broadway, R/PSD3, Boulder, CO, 80305-3337, USA
	Division	Department of Civil & Environmental Engineering & Earth Sciences
	Organization	University of Notre Dame
	Address	Notre Dame, IN, USA
	Email	andrey.grachev@noaa.gov
Author	Family Name	**Leo**
	Particle	
	Given Name	**Laura S.**
	Suffix	
	Division	Department of Civil & Environmental Engineering & Earth Sciences
	Organization	University of Notre Dame
	Address	Notre Dame, IN, USA
	Email	
Author	Family Name	**Sabatino**
	Particle	
	Given Name	**Silvana Di**
	Suffix	
	Division	Department of Civil & Environmental Engineering & Earth Sciences
	Organization	University of Notre Dame
	Address	Notre Dame, IN, USA
	Division	Department of Physics and Astronomy
	Organization	University of Bologna
	Address	Bologna, Italy
	Email	
Author	Family Name	**Fernando**
	Particle	
	Given Name	**Harindra J. S.**
	Suffix	
	Division	Department of Civil & Environmental Engineering & Earth Sciences

	Organization	University of Notre Dame
	Address	Notre Dame, IN, USA
	Email	
Author	Family Name	**Pardyjak**
	Particle	
	Given Name	**Eric R.**
	Suffix	
	Division	Department of Mechanical Engineering
	Organization	University of Utah
	Address	Salt Lake City, UT, USA
	Email	
Author	Family Name	**Fairall**
	Particle	
	Given Name	**Christopher W.**
	Suffix	
	Division	
	Organization	NOAA Earth System Research Laboratory
	Address	Boulder, CO, USA
	Email	

	Received	6 December 2014
Schedule	Revised	
	Accepted	28 April 2015

Abstract

Measurements of small-scale turbulence made in the atmospheric boundary layer over complex terrain during the Mountain Terrain Atmospheric Modeling and Observations (MATERHORN) Program are used to describe the structure of turbulence in katabatic flows. Turbulent and mean meteorological data were continuously measured on four towers deployed along the east lower slope (2–4 $_{\circ}$) of Granite Mountain near Salt lake City in Utah, USA. The multi-level (up to seven) observations made during a 30-day long MATERHORN field campaign in September–October 2012 allowed the study of temporal and spatial structure of katabatic flows in detail, and herein we report turbulence statistics (e.g., fluxes, variances, spectra, and cospectra) and their variations in katabatic flow. Observed vertical profiles show steep gradients near the surface, but in the layer above the slope jet the vertical variability is smaller. It is found that the vertical (normal to the slope) momentum flux and horizontal (along-slope) heat flux in a slope-following coordinate system change their sign below and above the wind maximum of a katabatic flow. The momentum flux is directed downward (upward) whereas the along-slope heat flux is downslope (upslope) below (above) the wind maximum. This suggests that the position of the jet-speed maximum can be obtained by linear interpolation between positive and negative values of the momentum flux (or the along-slope heat flux) to derive the height where the flux becomes zero. It is shown that the standard deviations of all wind-speed components (and therefore of the turbulent kinetic energy) and the dissipation rate of turbulent kinetic energy have a local minimum, whereas the standard deviation of air temperature has an absolute maximum at the height of wind-speed maximum. We report several cases when the destructive effect of vertical heat flux is completely cancelled by the generation of turbulence due to the along-slope heat flux. Turbulence above the wind-speed maximum is decoupled from the surface, and follows the classical local z-less predictions for the stably stratified boundary layer.

Keywords (separated by '-') Complex terrain - Horizontal heat flux - Katabatic flows - MATERHORN Program - Stable boundary layer

Footnote Information

Boundary-Layer Meteorol
DOI 10.1007/s10546-015-0034-8

RESEARCH ARTICLE

Structure of Turbulence in Katabatic Flows Below and Above the Wind-Speed Maximum

Andrey A. Grachev[1,2] · Laura S. Leo[2] · Silvana Di Sabatino[2,3] · Harindra J. S. Fernando[2] · Eric R. Pardyjak[4] · Christopher W. Fairall[5]

Received: 6 December 2014 / Accepted: 28 April 2015

Abstract Measurements of small-scale turbulence made in the atmospheric boundary layer over complex terrain during the Mountain Terrain Atmospheric Modeling and Observations (MATERHORN) Program are used to describe the structure of turbulence in katabatic flows. Turbulent and mean meteorological data were continuously measured on four towers deployed along the east lower slope (2–4°) of Granite Mountain near Salt lake City in Utah, USA. The multi-level (up to seven) observations made during a 30-day long MATERHORN field campaign in September–October 2012 allowed the study of temporal and spatial structure of katabatic flows in detail, and herein we report turbulence statistics (e.g., fluxes, variances, spectra, and cospectra) and their variations in katabatic flow. Observed vertical profiles show steep gradients near the surface, but in the layer above the slope jet the vertical variability is smaller. It is found that the vertical (normal to the slope) momentum flux and horizontal (along-slope) heat flux in a slope-following coordinate system change their sign below and above the wind maximum of a katabatic flow. The momentum flux is directed downward (upward) whereas the along-slope heat flux is downslope (upslope) below (above) the wind maximum. This suggests that the position of the jet-speed maximum can be obtained by linear interpolation between positive and negative values of the momentum flux (or the along-slope heat flux) to derive the height where the flux becomes zero. It is shown that the standard deviations of all wind-speed components (and therefore of the turbulent kinetic energy) and the dissipation rate of turbulent kinetic energy have a local minimum, whereas the standard deviation of air temperature has an absolute maximum at the height of wind-

✉ Andrey A. Grachev
andrey.grachev@noaa.gov

[1] NOAA Earth System Research Laboratory/Cooperative Institute for Research in Environmental Sciences, University of Colorado, 325 Broadway, R/PSD3, Boulder, CO 80305-3337, USA

[2] Department of Civil & Environmental Engineering & Earth Sciences, University of Notre Dame, Notre Dame, IN, USA

[3] Department of Physics and Astronomy, University of Bologna, Bologna, Italy

[4] Department of Mechanical Engineering, University of Utah, Salt Lake City, UT, USA

[5] NOAA Earth System Research Laboratory, Boulder, CO, USA

speed maximum. We report several cases when the destructive effect of vertical heat flux is completely cancelled by the generation of turbulence due to the along-slope heat flux. Turbulence above the wind-speed maximum is decoupled from the surface, and follows the classical local z-less predictions for the stably stratified boundary layer.

Keywords Complex terrain · Horizontal heat flux · Katabatic flows · MATERHORN Program · Stable boundary layer

1 Introduction

The local circulation in mountainous areas can in part be generated by vertical density gradients on sloped terrains (e.g., Whiteman 2000). During the nighttime overland in the mid-latitudes or at high latitudes the atmospheric boundary layer is often stably stratified, and on sloping terrain downslope flows (or katabatic flows) are generated above the surface. Katabatic flows are common over glaciers and ice sheets in Antarctica or Greenland.

A prominent feature of katabatic flow is a wind maximum close to the surface that causes a sign change in the momentum flux below and above the wind maximum. This obviously limits the application of traditional approaches for flux–profile relationships derived for the stable boundary layer (SBL) over flat surfaces where the vertical gradient of mean wind speed is considered to have the same sign. The downslope low-level jet is triggered by the positive vertical density gradient on a sloping surface, which also acts along the slope as katabatic forcing. Generally, the katabatic forcing term in the momentum budget equation is smaller than other terms (e.g., the background horizontal pressure gradient) and, for this reason, katabatic flows are generally observed during quiescent periods in the SBL. Under such conditions, katabatic flows efficiently drive the turbulent exchange of momentum, heat, moisture, and pollutants between the Earth's surface and the atmosphere. However, katabatic flows are poorly resolved in most numerical weather prediction, climate, and air pollution models because the typical jet maximum is located close to the Earth's surface.

Though much work has already been carried out on katabatic flows, a unified picture or theory does not exist. Several analytical models have been proposed, one of the first being the classical analytical solutions of Prandtl (1942), a case that Mahrt (1982) calls 'equilibrium flows'. Prandtl's approach has been extended to include time dependence, Coriolis effects, height-dependent eddy viscosity and diffusivity coefficients, etc. (e.g., Lykosov and Gutman 1972; Egger 1990; Papadopoulos et al. 1997; Ingel' 2000; Grisogono and Oerlemans 2001a, b; Grisogono 2003; Parmhed et al. 2004; Kavčič and Grisogono 2007; Stiperski et al. 2007; Shapiro and Fedorovich 2008; Grisogono and Zovko 2009; Axelsen et al. 2010; and references therein). Numerical weather prediction models have also been widely used to study katabatic flows (e.g., Renfrew 2004 and references therein). Denby (1999, Table I for a survey) described, 1.5-order and second-order closure models for turbulent kinetic energy (TKE) that have been used to study katabatic flow. A direct numerical simulation (DNS) of turbulent katabatic flows with and without the Coriolis effect was conducted by Shapiro and Fedorovich (2008) and Fedorovich and Shapiro (2009), while the development of large-eddy simulation (LES) models during the last few decades has enabled the simulation of boundary-layer flows such as the katabatic flow. Recently, Skyllingstad (2003), Smith and Skyllingstad (2005), Axelsen and Van Dop (2009a, b), and Grisogono and Axelsen (2012) have used LES to simulate katabatic flows (see a review of different LES by Smith and Porté-Agel 2013, their Table 1).

Journal: 10546-BOUN Article No.: 0034 TYPESET DISK LE CP Disp.:2015/5/2 Pages: 26 Layout: Small

Katabatic flows have a long history of investigation and the relevant literature is voluminous; they have been experimentally described covering various regions of the world, including the European Alps (e.g., Nadeau et al. 2013a, b; Oldroyd et al. 2014), Greece (Helmis and Papadopoulos 1996; Papadopoulos et al. 1997), Spain (Viana et al. 2010), the USA, Mountain States and south-west (e.g., Horst and Doran 1986, 1988; Neff and King 1987, 1988; Clements et al. 1989; Stone and Hoard 1989; Monti et al. 2002, 2014; Haiden and Whiteman 2005; Princevac et al. 2005, 2008; Whiteman and Zhong 2008; Pardyjak et al. 2009), Australia (Manins and Sawford 1979), and over glaciers and Polar ice caps and sheets (e.g., Meesters et al. 1997; Van den Broeke 1997; Smeets et al. 1998, 2000; Oerlemans et al. 1999; Van der Avoird and Duynkerke 1999; Denby and Smeets 2000; Oerlemans and Grisogono 2002; Renfrew and Anderson 2006; Zammett and Fowler 2007). A detailed review of the observational history of katabatic flows can be found in Poulos and Zhong (2008).

Limited observations still remain a problem for validation and calibration of katabatic flow models. In particular, during past field campaigns, turbulent measurements of katabatic flows were generally limited to a single flux tower equipped with one or two (and rarely more) levels of sonic anemometers. These conditions made for poor description of the turbulence structure of katabatic flows. The turbulence data collected in mountain terrain during the Mountain Terrain Atmospheric Modeling and Observations (MATERHORN) campaign offer several advantages for studying katabatic flows compared to previous field programs. These long-term, multi-level, multi-tower turbulent observations of the nocturnal SBL allow us to study the turbulence structure of the katabatic flows in detail. Here we report some results of turbulence measurements from the first MATERHORN field campaign (MATERHORN–Fall) carried out at the US Army Dugway Proving Grounds in Utah from 25 September through 31 October 2012 (Fernando et al. 2015).

2 The TKE Equation in a Slope-Following Coordinate System

Here we briefly describe the TKE equation. Unlike boundary layers over flat horizontal surfaces, the governing equations of the katabatic flow are described in a Cartesian coordinate system aligned with the slope, which is inclined at an angle $\alpha > 0$ to the horizontal (e.g., Denby 1999; Shapiro and Fedorovich 2008, 2014; Axelsen and Van Dop 2009a; Fedorovich and Shapiro 2009; Grisogono and Axelsen 2012; Łobocki 2014). The transformation from the traditional coordinate system where the vertical axis is aligned with the force of gravity to a slope-following coordinate system (i.e., rotation of the reference frame around the cross-slope axis by the slope angle α) can be accomplished by use of the metric tensor and the vector of the gravity field applied to the original equations (see details in Denby 1999, Eq. 18; Łobocki 2014, Appendix 2). In the current study, the katabatic flows are considered in a slope-following right-hand Cartesian coordinate system with axes directed, respectively, down the slope, across the slope, and perpendicular to the slope. Hereinafter, slope-normal and along-slope fluxes are associated with a slope-following (rotated) coordinate system whereas vertical (aligned with the gravity vector) and horizontal (normal to the gravity vector) are associated with a non-rotated coordinate system (if not stipulated specifically).

In a rotated coordinate system, the governing equations contain several modifications, in particular, the equation for downslope momentum contains the so-called katabatic forcing term associated with the temperature (density) perturbations (e.g., Mahrt 1982). As mentioned above, this term by definition drives the katabatic flow. Another important modification is associated with the TKE equation, which we consider in more detail since our study focuses

Journal: 10546-BOUN Article No.: 0034 TYPESET DISK LE CP Disp.:2015/5/2 Pages: 26 Layout: Small

on observations of small-scale turbulence. In a slope-following coordinate system, the TKE equation becomes (e.g., Horst and Doran 1988; Denby 1999; Łobocki 2014),

$$\partial \langle e \rangle / \partial t = -\langle u' w' \rangle \, (\partial U / \partial n) + \beta (\langle w' \theta'_v \rangle \cos \alpha - \langle u' \theta'_v \rangle \sin \alpha) - T - \varepsilon, \tag{1}$$

where $e = \left(u'^2 + v'^2 + w'^2\right)/2$ is the TKE, U is mean along-slope wind speed, n is the coordinate normal to the slope, ε is the dissipation rate of the TKE, θ_v is the virtual potential temperature, $\beta = g/\theta$ is the buoyancy parameter (g is the acceleration due to gravity and θ is the potential temperature), u, v, and w are the longitudinal (downslope), lateral (cross-slope), and vertical (normal) velocity components, respectively, [$'$] denotes fluctuations about the mean value, and $\langle\,\rangle$ is a time- or space-averaging operator. The transport and pressure work term in (1) is defined by $T = \partial \left(\langle w' e \rangle + \langle w' p' \rangle / \rho\right) / \partial n$ where p' is the fluctuation in atmospheric pressure and ρ is the air density.

In a slope-following coordinate system, the net buoyancy term in the TKE equation (Eq. 1) has an additional term $\langle u' \theta'_v \rangle \sin \alpha$ that is associated with the along-slope density flux tilted to the gravity vector. The net term $(\langle w' \theta'_v \rangle \cos \alpha - \langle u' \theta'_v \rangle \sin \alpha)$ in (1) is the sum of vertical components of the slope-normal and along-slope density fluxes (or temperature fluxes in the case of dry air). The modification of the buoyancy term in Eq. 1 leads to a modification of several stability parameters that contain this term; thus in a slope-following coordinate system, the flux Richardson number is (cf. Łobocki 2014, Eq. 23),

$$R_{\mathrm{f}} = -\frac{\beta (\langle w' \theta'_v \rangle \cos \alpha - \langle u' \theta'_v \rangle \sin \alpha)}{\langle u' w' \rangle \, (\partial U / \partial n)}. \tag{2}$$

The Monin–Obukhov stability parameter in a slope-following coordinate system is defined as the ratio of a reference height n normal to the slope and a modified Obukhov length scale L,

$$\zeta \equiv \frac{n}{L} = -\frac{n \, \kappa \beta (\langle w' \theta'_v \rangle \cos \alpha - \langle u' \theta'_v \rangle \sin \alpha)}{u_*^3}. \tag{3}$$

where the friction velocity $u_* = \left(\langle u' w' \rangle^2 + \langle v' w' \rangle^2\right)^{1/4}$ is considered positive below and above the wind maximum of slope flow. The von Kármán constant $\kappa \approx 0.4$ is included in Eq. 3 simply by convention. Discussion on the importance of the $\beta \langle u' \theta'_v \rangle \sin \alpha$ term to the Monin–Obukhov stability parameter (3) can also be found in Horst and Doran (1988, p. 615). Note that the sign of the $\sin \alpha$ factor in the buoyancy term in (1)–(3) depends on the direction of the along-slope axis (e.g., Shapiro and Fedorovich 2014, their Footnote 3). The sign is negative if the along-slope axis points down the slope (Horst and Doran 1988, and the current study) and vice versa (Denby 1999; Łobocki 2014).

The additional term $\beta \langle u' \theta'_v \rangle \sin \alpha$ in the TKE budget can enhance or suppress turbulence (depending on its sign, which will be discussed shortly), leading to a change in the critical gradient and flux Richardson numbers, which may not coincide with the canonical 'critical value' of 0.20 or 0.25 obtained for flat horizontal surfaces (see Grachev et al. 2013 for discussion). The critical value of the gradient and flux Richardson numbers for katabatic flows depends on the slope angle and the TKE budget (Horst and Doran 1988; Denby 1999). Near a local wind-speed maximum, the shear term becomes small and the gradient Richardson number can reach very high values, up to $Ri = 200$ (Smeets et al. 2000, their Fig. 4; Tse et al. 2003, their Fig. 3; Söderberg and Parmhed 2006, their Fig. 10).

The existence of a wind maximum in katabatic flows leads to a sign reversal of the momentum flux and along-slope heat flux at the wind-maximum height. For stably stratified flow over sloping terrain, the slope-normal gradient of mean potential temperature is positive throughout the entire layer, i.e., $\mathrm{d}\theta/\mathrm{d}n > 0$ (in the general case $\mathrm{d}\theta_v/\mathrm{d}n > 0$). However,

Journal: 10546-BOUN Article No.: 0034 TYPESET DISK LE CP Disp.:2015/5/2 Pages: 26 Layout: Small

the gradient of mean wind speed is positive ($\mathrm{d}U/\mathrm{d}n > 0$) below the wind maximum and it is negative ($\mathrm{d}U/\mathrm{d}n < 0$) above the wind maximum (obviously $\mathrm{d}U/\mathrm{d}n = 0$ at the wind-maximum height). To understand the vertical behaviour of the turbulent moments, we use physical arguments based on idealized turbulent eddy mixing. In the layer below the wind maximum, an upward moving air parcel ($w' > 0$) ends up being slower ($u' < 0$) and cooler ($\theta' < 0$) than its surroundings, while a downward ($w' < 0$) moving air parcel is faster ($u' > 0$) and warmer ($\theta' > 0$). We are assuming that particle temperature and velocity are conserved during its travel. Thus, in this region, both the upward and downward moving air parcels contribute negatively to both the $w\theta$ and uw covariances, that is, $\langle w'\theta'\rangle < 0$ and $\langle u'w'\rangle < 0$ respectively (meaning a downward transport of heat and momentum), but contribute positively to the along-slope heat flux, $\langle u'\theta'\rangle > 0$. However, the net fluid transport is zero ($\langle w\rangle = 0$) as expected from the equation of continuity. In the region above the slope-flow wind maximum ($\mathrm{d}U/\mathrm{d}n < 0$ and $\mathrm{d}\theta/\mathrm{d}n > 0$), an upward moving air parcel ($w' > 0$) is faster ($u' > 0$) and cooler ($\theta' < 0$) than its surroundings, while a downward ($w' < 0$) moving parcel is slower ($u' < 0$) and warmer ($\theta' > 0$), resulting in $\langle w'\theta'\rangle < 0$, $\langle u'w'\rangle > 0$, and $\langle u'\theta'\rangle < 0$ for both the upward and downward moving parcels.

Thus, the $\langle u'\theta_v'\rangle$ term is positive or downslope (a sink for TKE) below the wind-speed maximum and negative or upslope (a source for TKE) above. Because the slope-normal flux term $\langle w'\theta_v'\rangle$ is always negative under stable conditions (a sink for TKE), it is therefore the horizontal heat-flux term $\langle u'\theta_v'\rangle$ that increases (decreases) stability parameters (2) and (3) below (above) the wind-speed maximum. The contribution of the $\langle w'\theta_v'\rangle \cos\alpha$ term to the modified buoyancy term in the TKE equation decreases with slope angle, while the contribution of the $\langle u'\theta_v'\rangle \sin\alpha$ term increases with slope angle. In the case where

$$-\langle u'\theta_v'\rangle > -\cot\alpha\langle w'\theta_v'\rangle, \tag{4}$$

the net buoyancy term in Eq. 1 will be always positive even if the surrounding flow is stably stratified, that is, the above inequality implies a net positive buoyancy production of the TKE (recall that above the wind maximum both the slope-normal and along-slope heat fluxes are negative). Note that condition (4) is possible only in the region above the wind maximum and it is never reached below the wind maximum (see also field data presented in Sect. 4.1). The limit $\langle u'\theta_v'\rangle/\langle w'\theta_v'\rangle = \cot\alpha$ implies that the total heat-flux vector is perpendicular to the gravity vector (Denby 1999). In other words, a sink of TKE due to vertical buoyancy is completely cancelled by a source of TKE due to tilted along-slope buoyancy. Historically the inequality (4) was suggested and discussed by Denby (1999), who showed (p. 79) that Eq. 4 results in the critical angle $\alpha \approx 25°$ for $\langle u'\theta_v'\rangle/\langle w'\theta_v' >\approx 2.1$. A ratio of along-slope to slope-normal heat fluxes derived from the MATERHORN–Fall data are discussed further in Sect. 4. Discussion on the importance of the $\langle u'\theta_v'\rangle$ term in the other second-moment equations can be found in Horst and Doran (1988, p. 613).

Although in the layer above the wind maximum the kinematic momentum flux is negative, $\tau = -\langle u'w'\rangle < 0$ (upward momentum transfer), the production of turbulence by the mean flow shear in the TKE budget equation, $-\langle u'w'\rangle\,(\partial U/\partial n)$, and the turbulent viscosity, $K_m = -\frac{\langle u'w'\rangle}{\mathrm{d}U/\mathrm{d}n}$, are positive because both the momentum flux and gradient of mean wind speed change sign simultaneously. The change in the sign of the momentum flux for slope flows was theoretically and experimentally reported and discussed by Horst and Doran (1988), Neff (1990), Denby (1999), Denby and Smeets (2000), Söderberg and Tjernström (2004), Kouznetsov et al. (2013), Nadeau et al. (2013b), Monti et al. (2014), and Oldroyd et al. (2014).

Note that the phenomenon of upward momentum transfer is well known in air-sea interaction (e.g., Grachev and Fairall 2001 and references therein). Upward momentum transfer in the marine boundary layer (i.e., from water to air) can occupy the lowest 200 m of the atmospheric boundary layer (Smedman et al. 1994) and it is usually associated with fast-travelling swell running in the same direction as the wind or with decaying wind conditions. Such fast waves lead to a low-level wave-driven wind jet (Harris 1966); both this (e.g. Hanley and Belcher 2008, their Fig. 9) and a coastal jet (Brooks et al. 2003, their Figs. 3b and 8a) are very similar to a slope low-level jet, and one may expect that study of katabatic flows can be useful for the problem of the swell regime over oceans or jet-like structures, and vice versa.

Another issue is the transformation of the coordinate system in terms of measurements, considering that all theoretical results are derived in a slope-following coordinate system; however, theoretical or model findings are generally compared with experimental data obtained in both rotated and non-rotated coordinate systems (the current study is not an exclusion). For example, vertical gradients of air temperature/humidity or mean wind speed (measured by cup anemometers) are derived from sensors aligned with the force of gravity ("true" vertical line). Although the mean wind speed, direction, and turbulent wind stress are derived from a sonic anemometer, with double rotation of the anemometer axes needed to place the measured wind components in a terrain-following coordinate system (see details below), the origin of these vectors in the case of multi-level measurements are also located on a "true" vertical line ("mixed" coordinate system).

One can assume that for katabatic flows over gentle terrain, the discrepancy between measurements in a slope-following coordinate system and in a non-rotated coordinate system is insignificant and is within the accuracy of the experimental data. However, this difference may be substantial over very steep (e.g. $\alpha = 20°-40°$) slopes (cf. Geissbuhler et al. 2000; Van Gorsel et al. 2003; Nadeau et al. 2013a, b; Oldroyd et al. 2014), and we suggest that this intricacy should be taken into account in future field campaigns over steep slopes by modifying the experimental set-up. For example, 'slow' temperature and relative humidity probes, sonic anemometers, and other sensors can be aligned with a line normal to the slope using mounting arms/booms with different lengths (arms at upper levels should be longer than arms at lower levels) whereas a tower can still be aligned with the gravity vector. A length difference Δl of two arms located at different measurement levels should be $\Delta l = \Delta z \tan \alpha$ (if the arms are aligned with the "true" horizontal direction, that is, perpendicular to the tower) and $\Delta l = \Delta z \sin \alpha$ (if the arms are aligned with the slope) where Δz is the height difference between the two levels (in a non-rotated coordinate system) and α is the slope angle. Another issue is the azimuth and angle-of-attack dependent errors due to sensor orientation relative to the flow when the arms and/or sonic anemometers over a slope are aligned with the "true" horizontal direction (see Geissbuhler et al. 2000; Van Gorsel et al. 2003; Kochendorfer et al. 2012; Mauder 2013; Nadeau et al. 2013a for discussion).

3 The MATERHORN Observation Site and Instrumentation

The MATERHORN program is a five-year multi-disciplinary effort designed to better understand flow and turbulence process in mountainous terrain for improved mesoscale modelling and weather predictability. A comprehensive experimental part of the program focuses on field measurements for studying atmospheric processes over complex terrain (MATERHORN–X). The plans called for two major campaigns with high resolution measurements, with campaign periods selected based on the climatology of the area. The autumn campaign

Journal: 10546-BOUN Article No.: 0034 TYPESET DISK LE CP Disp.:2015/5/2 Pages: 26 Layout: Small

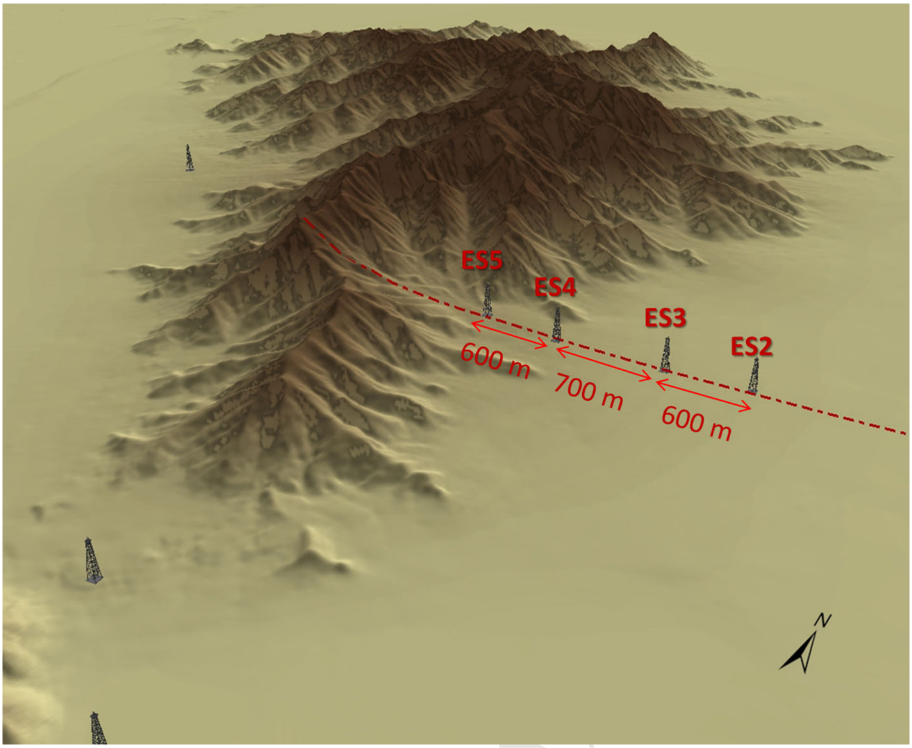

Fig. 1 Aerial view of the topography of Granite Mountain showing a schematic view of the experimental set-up at the east slope (towers ES2–ES5)

(MATERHORN–Fall, September–October 2012) focused on quiescent, dry, fair weather (wind speeds $<5\,\mathrm{m\,s^{-1}}$) periods dominated by diurnal heating and cooling, and the spring campaign (MATERHORN–Spring, May, 2013) sought measurements under highly variable synoptic conditions. Both MATERHORN–X field campaigns were carried out at the Granite Mountain Atmospheric Science Testbed (GMAST) of the Dugway Proving Grounds (DPG), a US Army facility, located approximately 140 km south-west of Salt Lake City, Utah in southern Tooele County and just north of Juab County. General information about the MATERHORN program and the field experiments can be found in Fernando et al. (2015).

Granite Mountain, an isolated topography within the DPG, is the centerpiece of the MATERHORN–X program; its length is 11.8 km, the largest width is 6.1 km, and peak elevation 0.84 km above the valley elevation (1.3 km above sea level). Granite Mountain was surrounded by several Intensive Observing Sites (IOS) including IOS-ES (east slope) and IOS-WS (west slope) to study slope flows, their interaction with valley flows, flow oscillations, and canyon effects. All IOS had heavily instrumented towers, with at least one 20-m tower at each IOS. To examine katabatic flows in detail, five towers designated as ES1–ES5 (IOS-ES) were placed along the fall line on the east slope of Granite Mountain and separated by about 600–700 m (Fig. 1).

The present study uses the data collected at IOS-ES (towers ES2–ES5 only) during the experiment MATERHORN–Fall in the autumn of 2012. The towers ES2–ES5 were instrumented with fast response three-axis sonic anemometer/thermometers that sampled at 20 Hz

Journal: 10546-BOUN Article No.: 0034 TYPESET DISK LE CP Disp.:2015/5/2 Pages: 26 Layout: Small

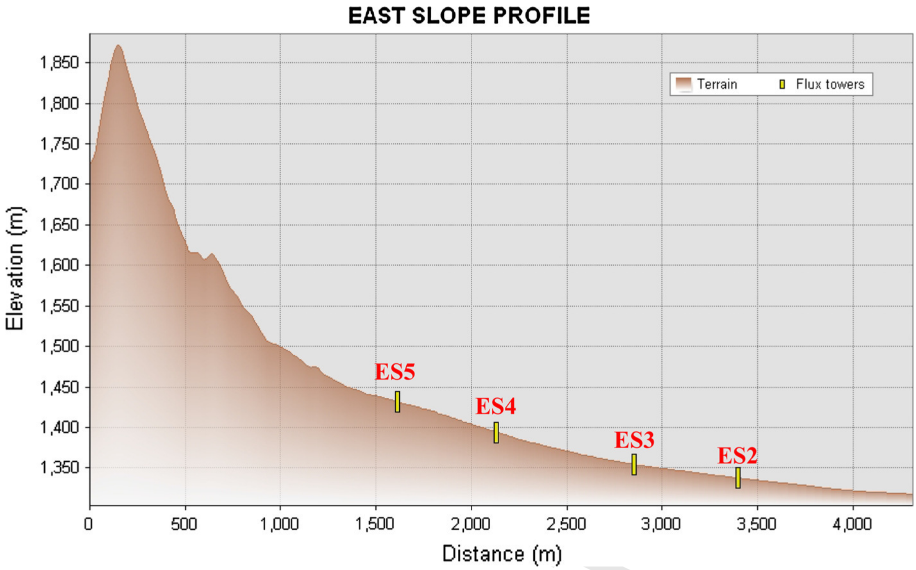

Fig. 2 Elevation cross-section at the location of the ES2–ES5 flux towers on the east slope of Granite Mountain

and slow response temperature and relative humidity (T/RH) probes that sampled at 1 Hz on the ES2 and ES3 towers and at 0.5 Hz on the ES4 and ES5 towers. Each flux tower at IOS-ES had several (at least five) levels of measurements. The sonic anemometers and the 'slow' Temperature and relative humidity probes were placed at seven levels on the ES2 tower (0.5, 4, 10, 16, 20, 25, and 28 m), at five levels on the ES3 tower (0.5, 2, 5, 10, and 20 m), at six levels on the ES4 tower (0.5, 2, 5, 10, 20, and 28 m), and at five levels on the ES5 tower (0.5, 2, 5, 10, and 20 m). The ES2 and ES4 towers were instrumented entirely with R.M. Young (Model 81000) sonic anemometers whereas the ES5 tower was instrumented entirely with Campbell Scientific, Inc. CSAT3 sonic anemometers. The ES3 tower was instrumented with a Campbell CSAT3 sonic anemometer and a fast response Campbell KH20 krypton hygrometer at the 2-m level and with R.M. Young sonic anemometers at other measurement levels. The towers were placed along the fall line on the east-facing slope of Granite Mountain (Fig. 1) with inclinations in the east-west direction ranging from approximately 2 to 4° and gradually increasing from ES2 to ES5 tower (Fig. 2).

The 'slow' probes provided air temperature and relative humidity measurements at several levels and were used to evaluate the vertical temperature and humidity gradients based on 30-min averaged 1-Hz data. The mean wind speed and wind direction were derived from the sonic anemometers, with rotation of the anemometer axes needed to place the measured wind components in a streamline coordinate system based on 30-min averaged 20-Hz data. We used the most common method, which is a double rotation of the anemometer coordinate system, to compute the longitudinal, lateral, and vertical velocity components in real time (Kaimal and Finnigan 1994, Sect. 6.6).

The 'fast' 20-Hz raw data measured by a sonic anemometer were first edited to remove spikes from the data stream. Turbulent covariance and variance values were then derived through the frequency integration of the appropriate cospectra and spectra computed from 27.31-min data blocks (corresponding to 2^{15} data points) from the original 30-min data files.

Journal: 10546-BOUN Article No.: 0034 TYPESET DISK LE CP Disp.:2015/5/2 Pages: 26 Layout: Small

In addition, to separate the contributions of mesoscale motions from the calculated eddy-correlation flux, a low-frequency cut-off at 0.0076 Hz (the tenth spectral value or a period of about 2 min) was applied on the cospectra as a lower limit of integration (see spectra and cospectra plots in Sect. 4.2); the upper limit of integration is 10 Hz (the Nyquist frequency). The low-frequency cut-off for turbulent contributions is chosen to lie in the spectral gap between the small-scale and large-scale contributions to the total transport (see Grachev et al. 2013, 2015 for details).

The dissipation rate of TKE (ε) in Eq. 1 was estimated based on a common method for measuring ε in a turbulent flow that assumes the existence of an inertial subrange associated with the Richardson–Kolmogorov cascade. The frequency energy spectrum of the longitudinal velocity component, $S_u(f)$, in the inertial subrange has the form,

$$S_u(f) = \alpha_K \, (U/2\pi)^{2/3} \, \varepsilon^{2/3} f^{-5/3}, \tag{5}$$

where f is the frequency, U is mean wind speed, and α_K is the Kolmogorov constant with an estimated value of $\alpha_K \approx 0.5{-}0.6$ (e.g. Kaimal and Finnigan 1994); a value $\alpha_K = 0.55$ is adopted for the current study. If the turbulence is locally isotropic, the spectral density of lateral and vertical velocity components are 4/3 of the longitudinal velocity, that is,

$$S_v(f) = S_w(f) = (4/3)\, S_u(f). \tag{6}$$

Based on (5) and (6), we derived ε separately from the spectra for each velocity component (u', v', and w') in the frequency domain 0.9–2.7 Hz (between the 50th and 61st spectral values) located within the inertial subrange. The median of these three values is taken as the representative dissipation rate. With this procedure, the influence of possible spectral spikes on the estimation of the dissipation rate and reduced sampling error is averted (see Grachev et al. 2015 and references therein for discussion). Because our estimates of ε are based on Eqs. 5 and 6, data without the Richardson–Kolmogorov cascade should be filtered out. In the current study, the following prerequisite is imposed on the data. The data points where the spectral slope in the inertial subrange (in the frequency domain 0.9–2.7 Hz) deviated more than 20 % of the theoretical $-5/3$ slope were excluded from the analysis (cf. Hartogensis and De Bruin 2005, where ±20 % was also used).

Similarly, the dissipation (destruction) rate for half the temperature variance, N_t, was derived from the $-5/3$ Obukhov-Corrsin power law for a passive scalar

$$S_t(f) = \beta_K \, (U/2\pi)^{2/3} \, N_t \varepsilon^{-1/3} f^{-5/3}, \tag{7}$$

where β_K is the Kolmogorov (Obukhov–Corrsin) constant for a passive scalar; a value of $\beta_K = 0.8$ (e.g., Kaimal and Finnigan 1994) is used in the current study. The dissipation rate of turbulent kinetic energy ε in Eq. 7 is estimated first from Eqs. 5 and 6 as described above.

4 Observed Turbulent Structure of Katabatic Flows

This paper concerns only those flows that resemble "pure" katabatic flows simultaneously at all ES2–ES4 flux towers, meaning that all profiles have a low-level wind maximum. Our observations during MATERHORN–Fall show that the katabatic flows are associated with quiescent synoptic conditions and generally clear skies; these flows are remarkably unidirectional and their duration can reach 2–3 h. It is found that the katabatic flows on the east slope of Granite Mountain ("slope flows") are rather intermittent and often disturbed due to strong interaction between the slope flows and the circulation in the Dugway valley

Journal: 10546-BOUN Article No.: 0034 TYPESET DISK LE CP Disp.:2015/5/2 Pages: 26 Layout: Small

occurring at various times during the night (Hocut et al. 2015). The westerly slope flows develop rapidly soon after sunset when the surface starts to cool; they persist for more than 2 h, interrupt, arise again, and decay at dawn.

Although episodes of the katabatic flows over the east slope occur quite often, only six cases of persistent westerly katabatic winds observed during the three nights of 28 and 30 September and 2 October 2012 [day of year (YD) = 272, 274, and 276] are analyzed in the current study. During these nights, the episodes of katabatic flow are observed at all ES2–ES4 flux towers from about 0200 to 0400 UTC and from 0530 to 0630 UTC (local time 2000 to 2200 and from 2330 to 0030 of a previous day for the most part). Note that the local time in Utah during the experiment MATERHORN–Fall is UTC minus 6 h, that is, the local time zone is US Mountain Daylight Time (MDT). All times hereinafter are time stamped to reflect a 30-min data file; e.g. a date time 0200 indicates that data were collected and averaged from 0200 until 0230.

We suggest that the identical time periods of the observed katabatic winds on the east slope of Granite Mountain during these nights may characterize a universal pattern of nocturnal circulation at the Dugway basin for similar conditions. During these time periods the downslope flows appears to be free from interactions with the valley circulation.

4.1 Vertical Profiles of Turbulence Quantities

We next consider one of the six episodes of the katabatic flows mentioned above (YD 272, 0200–0400 UTC) in detail (other episodes are also analyzed in the coming sections). Figures 3 and 4 show vertical (normal to a slope) profiles of the 30-min average wind speed, air temperature, turbulent fluxes, standard deviation of the sonic temperature, TKE energy, and dissipation rate of TKE observed at the ES3 flux tower on the east slope of Granite Mountain for four different time periods during the night of 28 September 2012 (YD 272, 0200–0400 UTC); local time is from 2000 to 2200 of the previous day, 27 September 2012. In Fig. 5 we compare the average profiles of mean wind speed, the downwind stress (momentum flux), and standard deviation of air temperature measured at the ES4 tower with their counterparts observed at the ES3 tower for the same time periods (Figs. 3, 4). Moreover, Fig. 5d shows slope-normal profiles of the dissipation (destruction) rate for half the temperature variance, N_t, observed at the ES4 tower. Unlike the plots in Figs. 3, 4 and 5, where the temporal evolution of turbulence profiles at the ES3 and ES4 towers are presented (using an Eulerian description of the slope flow), Fig. 6 shows spatial behaviour of the vertical profiles of the 30-min average wind speed and turbulent fluxes along the slope at the four ES2–ES5 flux towers for the specific time period YD 272, 0300 UTC (2-D description). Turbulent fluxes and variances in Figs. 3, 4, 5, 6 and 7 are computed through frequency integration over the high-frequency parts of the appropriate spectra and cospectra (with about a 2-min cut-off time scale as the low-pass filter) that are associated with energy-containing, flux-carrying eddies (see Sect. 3). Turbulent quantities based on the high-frequency parts of the spectra and cospectra provide somewhat smaller scatter of the data as compared to their 30-min average counterparts.

The vertical profiles of the downslope wind-speed component from all sites (Figs. 3a, 5a, 6a) show a typical "pure" katabatic flow structure with the wind-speed maximum located between heights of 3 and 5 m. Figure 3b shows a typical vertical profile of air temperature measured by the 'slow' temperature and humidity probes. Note the slow cooling of the air layer for four different time periods during 0200–0330 UTC (Fig. 3b). During the time covered by Fig. 3, relative humidity at ES3 tower monotonically decreases from 30 to 36 % at the 0.5-m measurement level to 23–25 % in the layer 10–20 m (not shown).

Journal: 10546-BOUN Article No.: 0034 TYPESET DISK LE CP Disp.:2015/5/2 Pages: 26 Layout: Small

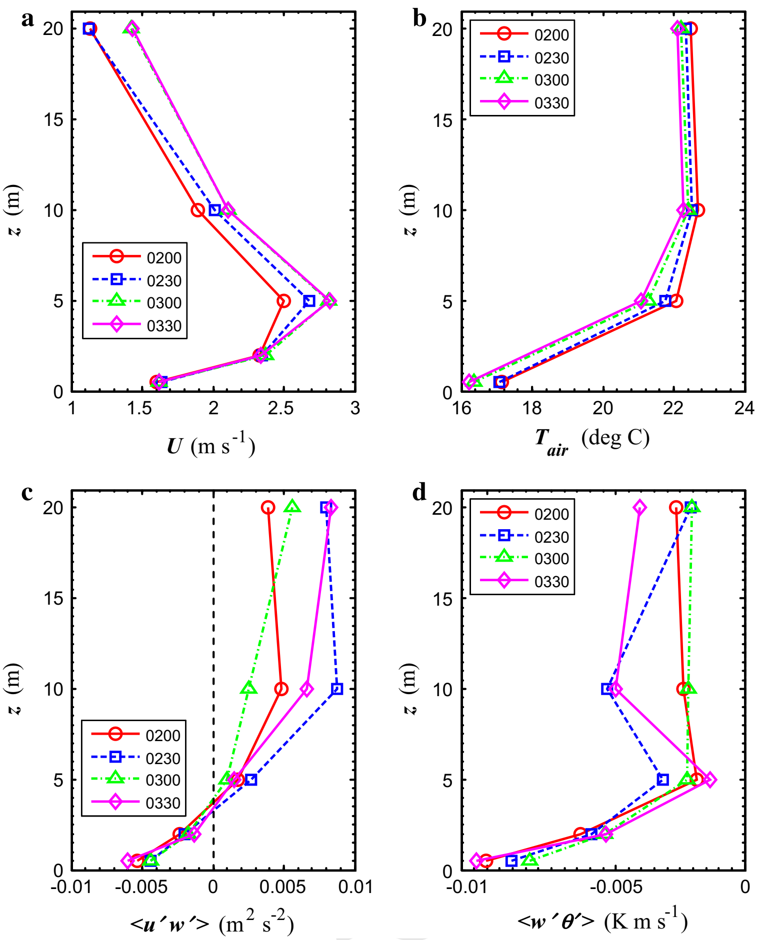

Fig. 3 Plots of vertical profiles of the **a** wind speed, **b** air temperature (level 2 is missing), **c** $\langle u'w' \rangle$, **d** $\langle w'\theta' \rangle$ observed at the ES3 flux tower on the east slope of Granite Mountain on 28 September 2012 (YD 272, 0200–0330 UTC)

According to Figs. 3, 4, 5 and 6, the profiles of velocity, turbulent fluxes, and other quantities show steep gradients in the layer below the wind-speed maximum. Obviously in this region the concept of the constant-flux layer is invalid for momentum and heat fluxes. However above the slope jet, the wind speed, temperature, turbulent fluxes, and variances vary with height more slowly than near the surface (approximately an order of magnitude). In the region of a wind-speed maximum, a local minimum is found for the TKE, $\langle e \rangle = \left(\sigma_u^2 + \sigma_v^2 + \sigma_w^2\right)/2$, (Fig. 4c) and the dissipation rate of TKE (Fig. 4d), whereas the standard deviation of the sonic temperature, σ_t, has an absolute maximum near the wind-speed maximum (Figs. 4b, 5c). Although this behaviour in TKE and σ_t has been previously predicted by Horst and Doran (1988), Denby (1999, Figs. 3, 4), and Söderberg and Parmhed (2006), a reliable experimental verification for katabatic flows has been lacking. The dissipation (destruction) rate for half the temperature variance, N_t, derived from Eq. 7 generally decreases monotonically with height, although several cases of a weak local maximum near a wind-speed maximum were found (Fig. 5d).

Journal: **10546-BOUN** Article No.: **0034** TYPESET DISK LE CP Disp.:**2015/5/2** Pages: **26** Layout: **Small**

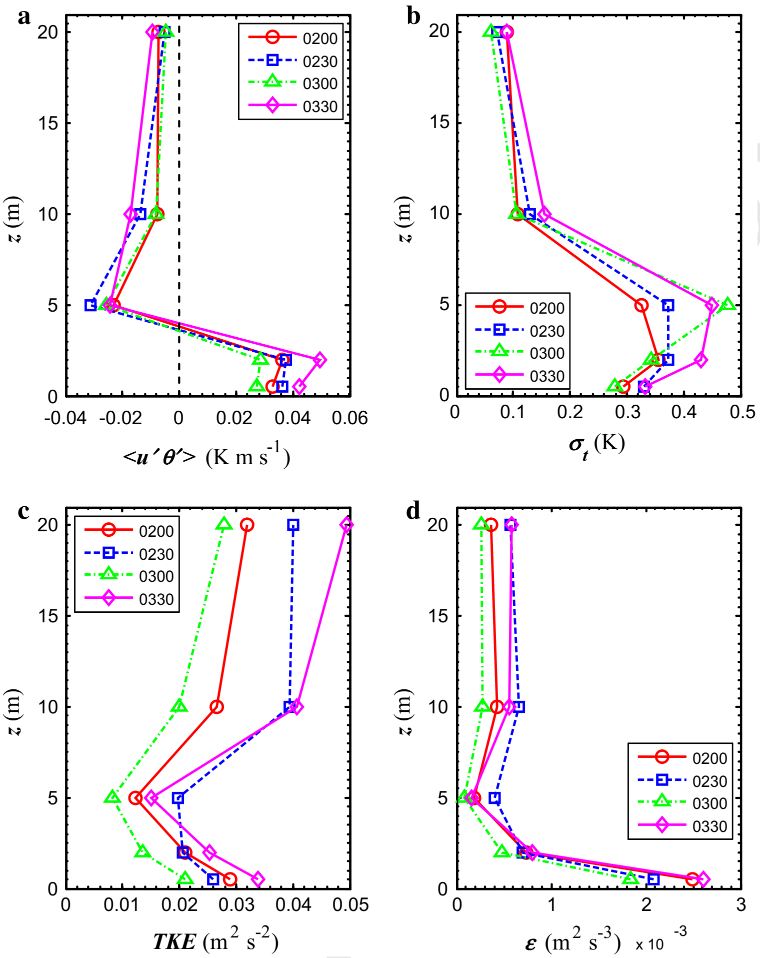

Fig. 4 Plots of vertical profiles of the **a** $\langle u'\theta'\rangle$, **b** standard deviation of the air temperature, σ_t, **c** turbulent kinetic energy (TKE), **d** dissipation rate of TKE, ε, observed at the ES3 flux tower on 28 September 2012 (YD 272, 0200–0330 UTC)

In the case of a nocturnal low-level jet (LLJ), Banta et al. (2006) and Pichugina and Banta (2010) reported the minimum in σ_u^2 (and TKE) at the LLJ nose observed by high resolution Doppler lidar. The minimum in TKE at the jet nose results from $\partial U/\partial n$ becoming zero at this level, as noted by Banta et al. (2006, p. 2716). Although the shear production term $\langle u'w'\rangle\,(\partial U/\partial n) = 0$ at the level of the wind-speed maximum, it is not necessarily true that TKE tends to zero there, or that no vertical mixing occurs through this level. Data in the present study and in Banta et al. (2006) indicate that TKE (or σ_u^2) and ε became small but remained non-zero at the height of the wind-speed maximum.

As mentioned earlier in Sect. 2, a striking feature of katabatic flows is a sign reversal of the vertical momentum flux (downslope stress), $\tau = -\langle u'w'\rangle$, and the along-slope temperature (heat) flux, $\langle u'\theta_v'\rangle$, at the wind-maximum height. Observed profiles of $\langle u'w'\rangle$ and $\langle u'\theta'\rangle$ over the east slope of Granite Mountain are shown in Figs. 3c, 5b, 6b and Figs. 4a, 6d respectively.

Journal: 10546-BOUN Article No.: 0034 TYPESET DISK LE CP Disp.:2015/5/2 Pages: 26 Layout: Small

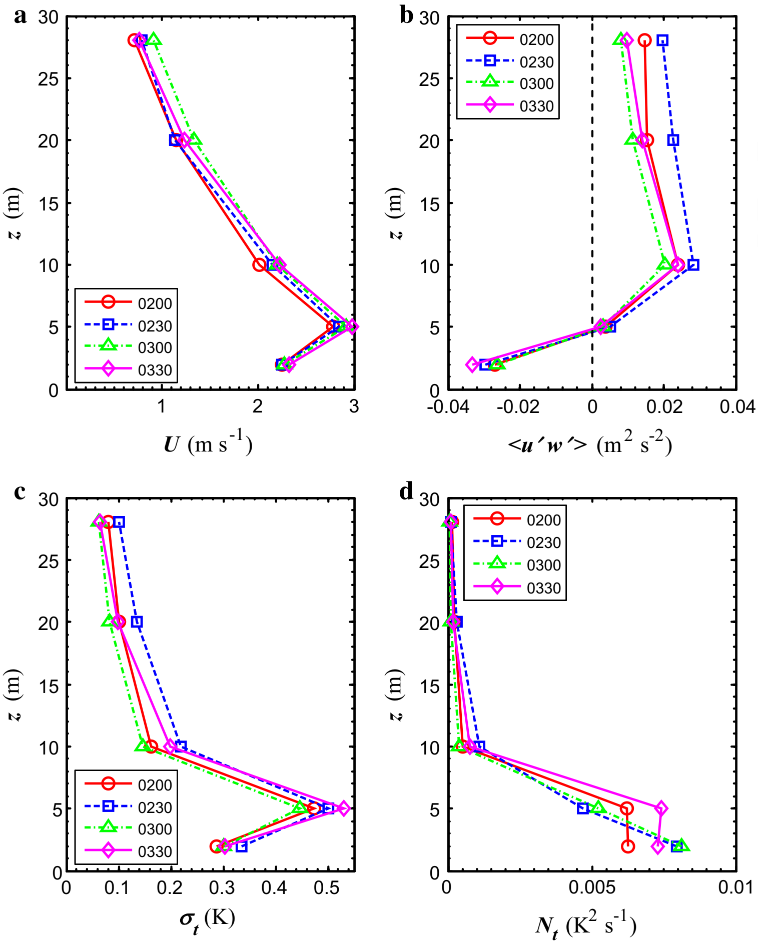

Fig. 5 Plots of vertical profiles of the **a** wind speed, **b** $\langle u'w' \rangle$, **c** standard deviation of the air temperature, σ_t, **d** dissipation (destruction) rate for half the temperature variance observed at the ES4 flux tower (level 1 is missing) on 28 September 2012 (YD 272, 0200–0330 UTC)

According to our data, $\langle u'w' \rangle$ is negative (positive) whereas $\langle u'\theta' \rangle$ is positive (negative) below (above) the wind-speed maximum. In other words, the vertical momentum flux is directed downward (upward) whereas the along-slope temperature flux is downslope (upslope) below (above) the wind-speed maximum in a slope-following coordinate system. Therefore, we suggest that the position of the jet-speed maximum can be derived from Figs. 3, 4, 5 and 6 using the intersection of linearly interpolated lines for positive and negative values of $\langle u'w' \rangle$ or $\langle u'\theta'_v \rangle$ with a vertical line (see the next section for details).

According to Figs. 3, 4 and 5, the vertical profiles of the wind speed and various turbulent quantities are approximately stationary in time (especially near the surface) for each specific tower (ES3 or ES4) during four different time periods for YD 272, 0200–0400 UTC. For example, vertical profiles of mean wind speed measured at the ES3 flux tower are almost identical for 0300 and 0330 (Fig. 3a). However, according to Fig. 6, the vertical profiles of the wind speed and turbulent fluxes along the flow line (from one tower to another)

Journal: 10546-BOUN Article No.: 0034 TYPESET DISK LE CP Disp.:2015/5/2 Pages: 26 Layout: Small

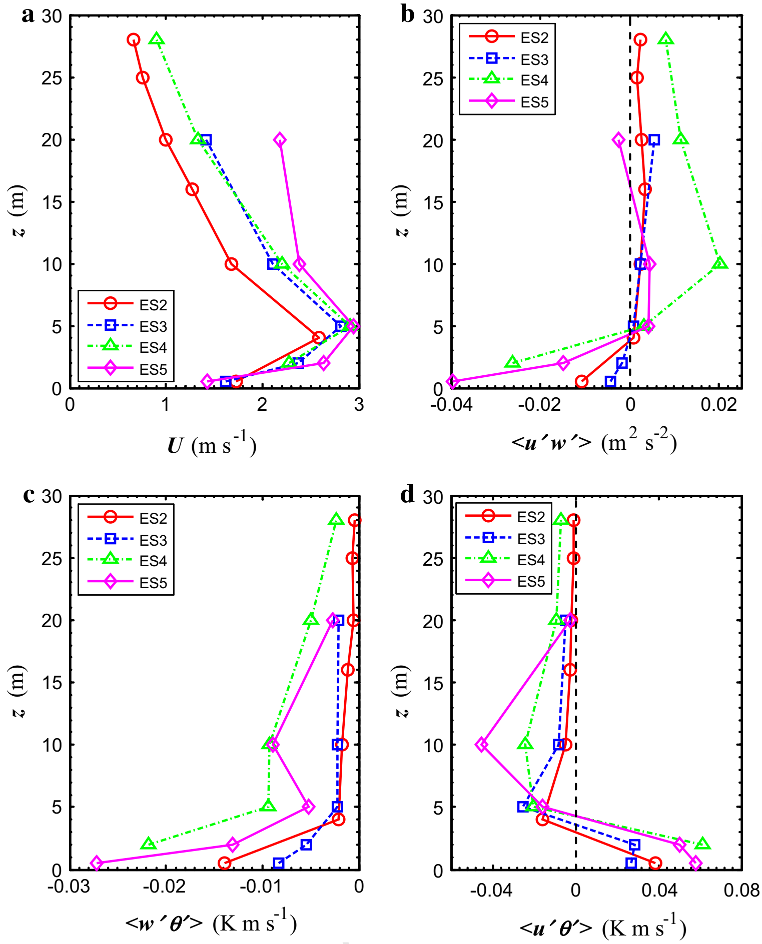

Fig. 6 Plots of vertical profiles of the **a** wind speed, **b** $\langle u'w' \rangle$, **c** $\langle w'\theta' \rangle$, **d** $\langle u'\theta' \rangle$ observed at the ES2, ES3, ES4, and ES5 flux towers on the east slope of Granite Mountain on 28 September 2012 (YD 272, 0300 UTC)

vary widely for a fixed time period (YD 272, 0300 UTC). Note that significantly higher momentum flux is observed at the ES4 tower (Figs. 5b, 6b), which may be associated with higher aerodynamic roughness near the ES4 location (e.g., boulders, bushes). Thus, surface values of the turbulent fluxes in katabatic flows vary along a slope due to different properties of the underlying surface. Remarkably, however, the surface fluxes are almost constant over time for a specific slope location, implying that the katabatic flow adapts readily to new surface conditions down the slope.

Since the along-slope heat (buoyancy) flux $\langle u'\theta_v' \rangle$ contributes to the net buoyancy term in the TKE budget equation, and observations of the along-slope heat flux are very limited in the literature, we consider its relative contribution to the buoyancy in more detail. Figure 7 shows the vertical profiles of the ratio $\langle u'\theta_v' \rangle / \langle w'\theta_v' \rangle$ measured at different towers on different days. According to Fig. 7, the ratio $\langle u'\theta_v' \rangle / \langle w'\theta_v' \rangle$ has a negative minimum (positive maximum) below (above) the wind-speed maximum (Fig. 7b–d). Although typical values of the positive maximum for this ratio range between 5 and 10, some values reach 13–19 (Fig. 7a–c). At

Journal: 10546-BOUN Article No.: 0034 TYPESET DISK LE CP Disp.:2015/5/2 Pages: 26 Layout: Small

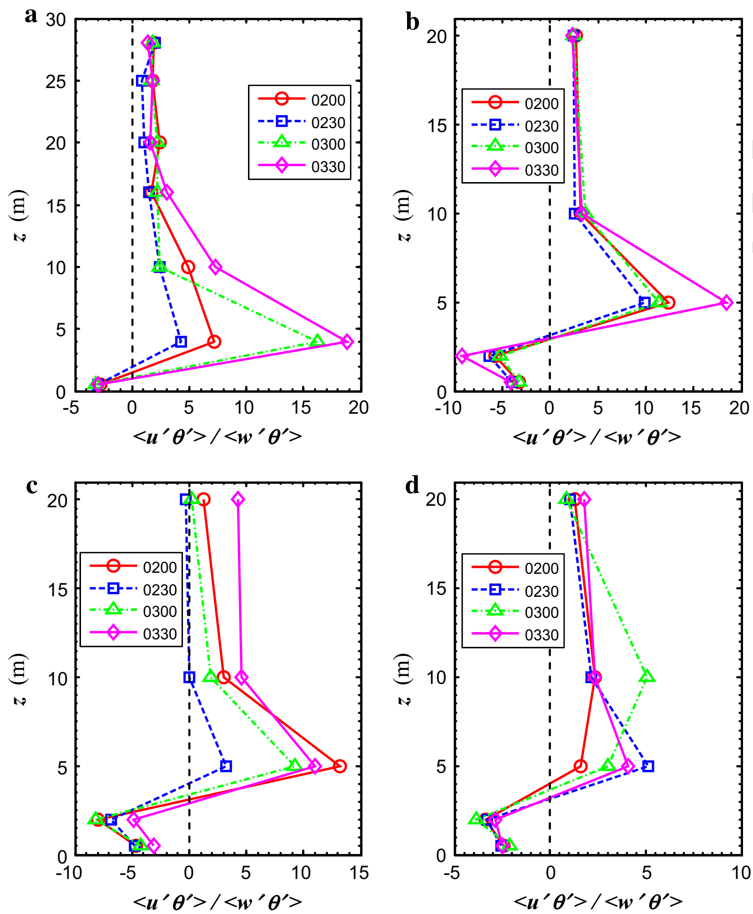

Fig. 7 Plots of vertical profiles of the ratio $\langle u'\theta'\rangle/\langle w'\theta'\rangle$ for **a** ES2 tower, YD 274, 0200–0330 UTC, **b** ES3 tower, YD 272, 0200–0330 UTC, **c** ES3 tower, YD 276, 0200–0330 UTC, **d** ES5 tower, YD 272, 0200–0330 UTC

the east slope of Granite Mountain values of $\cot\alpha$ range from 28.6 to 14.3 ($\alpha \approx 2$–$4°$), implying that the net buoyancy term $\beta\left(\langle w'\theta_v'\rangle\cos\alpha - \langle u'\theta_v'\rangle\sin\alpha\right)$ approximately equals zero for $\langle u'\theta_v'\rangle/\langle w'\theta_v'\rangle \approx 19$ or even the net buoyancy term changes a sign, see the inequality (4). Thus, our data provide experimental evidence that the along-slope heat (buoyancy) flux in a slope-following coordinate system plays a crucial role in the dynamics of the katabatic flow even over gentle slopes.

4.2 Analysis of Turbulence Spectra and Cospectra

Figure 8 shows typical raw cospectra for the downwind stress (momentum flux) and the along-slope flux of sonic temperature (kinematic along-slope sensible heat flux) at five levels (0.5, 2, 5, 10, and 20 m) for a case of a westerly katabatic flow observed at the ES3 flux tower on 28 September 2012 (YD 272, 0230 UTC); local time is 2030 of the previous day. True wind direction derived from the sonic anemometers is in the range 273–286° for all five

Journal: 10546-BOUN Article No.: 0034 TYPESET DISK LE CP Disp.:2015/5/2 Pages: 26 Layout: Small

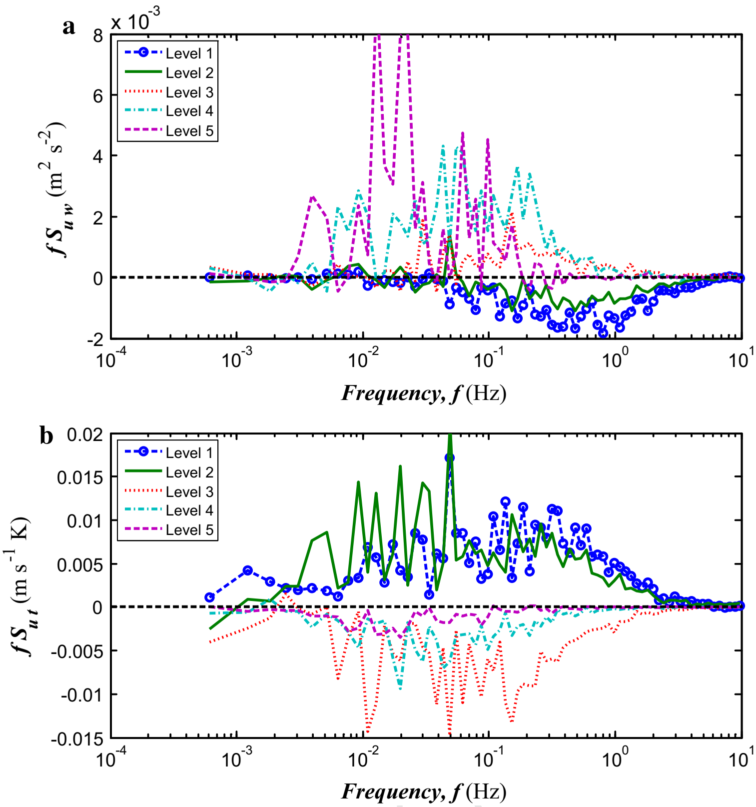

Fig. 8 Typical raw cospectra of **a** the downwind stress and **b** the along-slope flux of sonic temperature at five levels (0.5, 2, 5, 10, and 20 m) for a case of katabatic flow observed at the ES3 flux tower on the east slope of Granite Mountain on 28 September 2012 (YD 272, 0230 UTC); local time is 2030 of the previous day (local time zone is MDT). The cospectra are computed from 27.31-min data blocks (corresponding to 2^{15} data points). For data presented in the *upper panel* **a** the momentum flux $\langle u'w' \rangle \approx -0.0044, -0.0024, 0.0033, 0.0095, 0.0094\,\mathrm{m^2\,s^{-2}}$ for the levels from 1 to 5. For data presented in the *bottom panel* **b** the along-slope flux of sonic temperature $\langle u'\theta' \rangle \approx 0.0430, 0.0395, -0.0407, -0.0162, -0.0062\,\mathrm{K\,m\,s^{-1}}$ for the levels from 1 to 5. Note that the levels 1 and 2 are located below the wind-speed maximum whereas the levels 3–5 are located above the wind-speed maximum. The slope-normal flux of sonic temperature $\langle w'\theta' \rangle \approx -0.0089, -0.0058, -0.0039, -0.0058, -0.0023\,\mathrm{K\,m\,s^{-1}}$ for the levels from 1 to 5 (cospectra of $\langle w'\theta' \rangle$ are not shown). Additional information about this case can be found in Figs. 3 and 4

levels. The frequency-weighted cospectra in Fig. 8 are in log-linear coordinates, so that the area under the spectral curve represents the total covariance.

According to Fig. 8, the momentum flux and the along-slope sensible heat flux change their sign between heights of 2 m (level 2) and 5 m (level 3); in particular, the momentum flux is directed downward (upward) below (above) the wind-speed maximum (cf. Smeets et al. 2000, their Fig. 4). As discussed earlier, this is associated with the fact that levels 1 and 2 are located below a wind-speed maximum whereas levels 3–5 are located above a wind-speed maximum. This is consistent with the vertical profile of the mean wind speed ≈1.64, 2.34, 2.68, 2.01 and $1.12\,\mathrm{m\,s^{-1}}$ (the levels from 1 to 5 respectively) for the case shown in Fig. 8 (see also Fig. 3a). Therefore, we suggest deriving a position of the wind-speed maximum from linear interpolation between positive and negative values of the momentum flux (or

Journal: 10546-BOUN Article No.: 0034 TYPESET DISK LE CP Disp.:2015/5/2 Pages: 26 Layout: Small

along-slope heat flux). A height of the wind-speed maximum H_{max} corresponds to a level where the fluxes $\langle u'w'\rangle$ and $\langle u'\theta'\rangle$ become zero. Based on the values of $\langle u'w'\rangle$ and $\langle u'\theta'\rangle$ for Fig. 8, linear interpolation of the momentum flux between levels 2 and 3 gives $H_{max} \approx 3.3$ m whereas linear interpolation of the along-slope heat flux leads to $H_{max} \approx 3.5$ m (mean value for both methods $H_{max} \approx 3.4$ m). It is clear that the flux-interpolation method gives more accurate estimates of H_{max} than a method based on measurements of the vertical profile of the mean wind speed. In our case, the method based on the wind-speed profile leads to H_{max} located somewhere between 2 and 5 m. Note that an interpolation method can be applied only to variables that change sign at the level of the wind-speed maximum.

Figure 9 shows typical one-dimensional, raw energy spectra of the longitudinal, lateral, and vertical velocity components computed in a slope-following coordinate system, and the sonic temperature for a case of a westerly katabatic flow observed at a flux tower, levels 2–6 (2, 5, 10, 20, and 28 m; level 1 at 0.5 m is missing), 28 September 2012 (YD 272, 0330 UTC); local time is 2130 of the previous day. The vertical profile of the mean wind speed for the case shown in Fig. 6 is ≈2.32, 2.98, 2.22, 1.24, and 0.76 $\mathrm{m\,s^{-1}}$ (the levels from 2 to 6 respectively). True wind direction derived from the sonic anemometers is in the range 276–285° for all five levels.

The case shown in Fig. 9 is interesting because the measurement level 3 located at 5 m is close to a wind-speed maximum. For this case (Fig. 9), the momentum flux $\langle u'w'\rangle$ equals $\approx -0.0337, 0.0016, 0.0237, 0.0158, 0.0130\,\mathrm{m^2\,s^{-2}}$ for the levels from 2 to 6; the vertical flux of sonic temperature $\langle w'\theta'\rangle \approx -0.0278, -0.0117, -0.0132, -0.0059, -0.0037\,\mathrm{K\,m\,s^{-1}}$ for the levels from 2 to 6; the along-slope flux of sonic temperature $\langle u'\theta'\rangle \approx 0.0684, -0.0098, -0.0491, -0.0209, -0.0119\,\mathrm{K\,m\,s^{-1}}$ for the levels from 2 to 6. Accordingly, level 2 is located below a wind-speed maximum whereas levels 4–6 are located above it. Turbulent fluxes $\langle w'u'\rangle$ and $\langle u'\theta'\rangle$ at measurement level 3 are close to zero, and thus this level is located close to a wind-speed maximum (slightly above). The height of the wind-speed maximum H_{max} based on linear interpolation of the momentum flux between levels 2 and 3 gives $H_{max} \approx 4.9$ m whereas linear interpolation of the along-slope heat flux leads to $H_{max} \approx 4.6$ m (mean value for both methods $H_{max} \approx 4.7$ m).

According to Fig. 9, the turbulent spectral curves have a wide inertial subrange, which displays the $-5/3$ Kolmogorov power law for velocity components (the Obukhov-Corrsin law for the passive scalar) at high frequencies (a slope of $-2/3$ for the frequency-weighted spectra plotted in Fig. 9) at all five sonic levels 2–6. Although in the layer above the wind maximum (levels 3–6) the momentum flux is negative, $\tau = -\langle u'w'\rangle < 0$ (upward momentum transfer) and moreover at level 3 the production of TKE $-\langle u'w'\rangle\,(\partial U/\partial n) \approx 0$, the turbulence here is still associated with the Richardson–Kolmogorov cascade (Fig. 9). Additional plots of the spectra and cospectra for katabatic winds can be found in Smeets et al (2000, Fig. 4).

According to the spectra plots in Fig. 9, the standard deviations of all wind-speed components (and therefore TKE) have a local minimum (cf. Fig. 4c), whereas the standard deviation of the air temperature σ_t has an absolute maximum at the height of the slope wind maximum H_{max} (cf. Fig. 4b, 5c). Figures 8 and 9 also generally support the conclusion that the turbulent fluxes and variances in the layer below the wind-speed maximum vary with height more rapidly (approximately an order of magnitude) than in the layer above the slope jet.

4.3 Local z-Less Stratification

In the region of the wind-speed maximum, production of turbulence by wind shear is quite small or even zero at this maximum where $\langle u'w'\rangle = 0$ and a local minimum in TKE and ε (Fig. 4c, d) is observed. This suggests that turbulent exchange across the wind-speed

Journal: 10546-BOUN Article No.: 0034 TYPESET DISK LE CP Disp.:2015/5/2 Pages: 26 Layout: Small

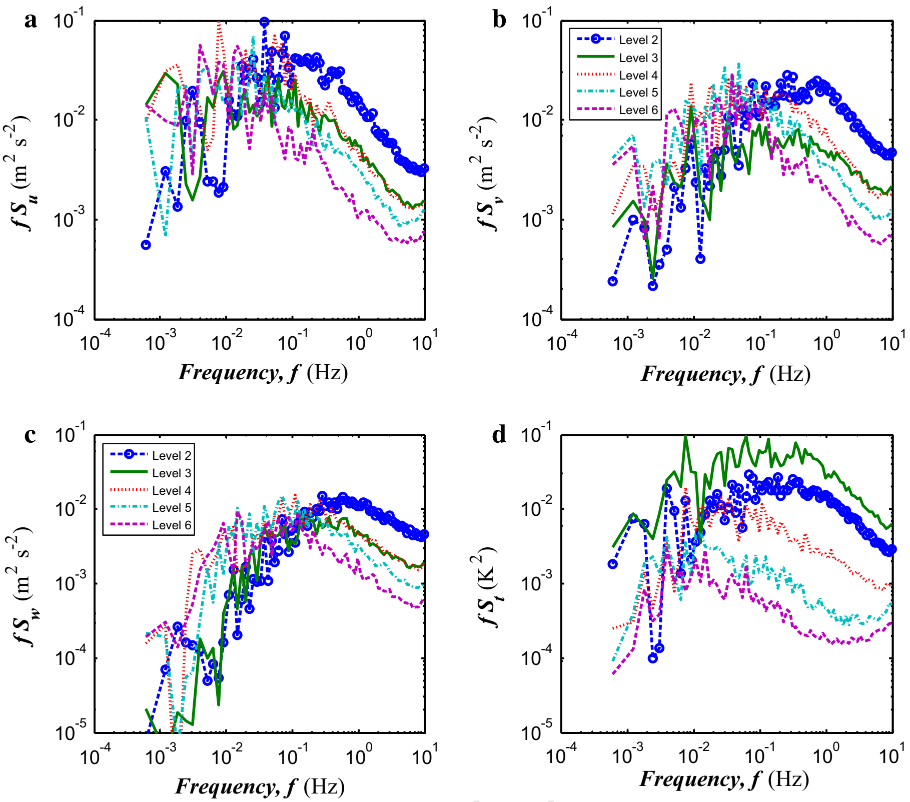

Fig. 9 Typical raw energy spectra of the **a** longitudinal, **b** lateral, and **c** vertical velocity components and **d** the sonic temperature for a case of katabatic flow observed at the ES4 flux tower, levels 2–6 (2, 5, 10, 20, and 28 m; level 1 at 0.5 m is missing), 28 September 2012 (YD 272, 0330 UTC); local time is 2130 of the previous day (local time zone is MDT). The spectra are computed from 27.31-min data blocks (corresponding to 2^{15} data points). For the spectra shown, the standard deviation of the longitudinal wind speed component $\sigma_u \approx 0.4144$, 0.3538, 0.4391, 0.3614, and 0.3550 m s^{-1} (levels from 2 to 6 respectively), the standard deviation of the lateral wind speed component $\sigma_v \approx 0.2944$, 0.1983, 0.2952, 0.2887, and 0.2459 m s^{-1} (levels from 2 to 6 respectively), the standard deviation of the vertical wind-speed component $\sigma_w \approx 0.2137$, 0.1650, 0.2048, 0.1926, and 0.1571 m s^{-1} (levels from 2 to 6 respectively), and the standard deviation of the sonic temperature $\sigma_t \approx 0.3291$, 0.5592, 0.2069, 0.1157, and 0.0794 K (levels from 2 to 6 respectively). Note that the level 2 is located below the wind-speed maximum whereas the levels 4–6 are located above a wind-speed maximum. The measurement level 3 is close to the wind-speed maximum

maximum ceases and the turbulence above the slope jet can be largely decoupled from the flow below and from the underlying surface (Horst and Doran 1988; Denby 1999). Thus, in this region, the turbulence no longer communicates effectively with the surface and various quantities become independent of the height of measurement z (or n), that is z (or n) ceases to be a scaling parameter. This limit was termed 'z-less stratification' (height-independent) by Wyngaard and Coté (1972). Note that the difference between z and $n = z \cos\alpha$ in our case is negligible (less than 1 %), and so $n \approx z$ and $\zeta = n/L \approx z/L$, Eq. 3, in the current study.

We tested the classical local z-less predictions for the Monin–Obukhov non-dimensional functions φ_m, φ_ε, and φ_α in the layer above the slope jet. The non-dimensional vertical gradient of the mean wind speed, U, and the non-dimensional dissipation rate of TKE ε according to Monin–Obukhov similarity theory (MOST) are expressed as,

$$\phi_m(\zeta) = -\left(\frac{\kappa n}{u_*}\right)\frac{\mathrm{d}U}{\mathrm{d}n}, \tag{8}$$

$$\phi_\varepsilon(\zeta) = \frac{\kappa n \varepsilon}{u_*^3}, \tag{9}$$

noting that the function $\phi_m > 0$ above a wind-speed maximum. The standard deviations of wind-speed components σ_α are scaled as

$$\phi_\alpha(\zeta) = \frac{\sigma_\alpha}{u_*}, \tag{10}$$

where $\alpha (= u, v,$ and $w)$ denotes the longitudinal, lateral, or vertical velocity component, the friction velocity is computed as $u_* = \left(\langle u'w'\rangle^2 + \langle v'w'\rangle^2\right)^{1/4}$, and $\zeta = n/L$ is defined by (3). The z-less concept requires that n cancels in Eqs. 8–10, which corresponds to

$$\varphi_m(\zeta) = \beta_m \zeta, \tag{11}$$

$$\varphi_\varepsilon(\zeta) = \beta_\varepsilon \zeta, \tag{12}$$

$$\varphi_\alpha(\zeta) = \beta_\alpha, \tag{13}$$

where β_m, β_ε, and β_α are numerical coefficients. A simple linear interpolation $\varphi_m(\zeta) = 1 + \beta_m \zeta$ and $\varphi_\varepsilon(\zeta) = 1 + \beta_\varepsilon \zeta$ has been suggested to provide blending between neutral and very stable (‘z-less’) cases.

Figure 10 shows plots of the normalized standard deviations of all three wind-speed components defined by Eq. 10 (local scaling). According to Fig. 10, the universal functions $\varphi_\alpha(\zeta)$ are approximately constant, that is, they are consistent with the classical Monin–Obukhov z-less prediction (13). The horizontal dashed lines in Fig. 10 correspond to $\beta_u = 2.3$, $\beta_v = 2.0$, and $\beta_w = 1.5$, which are median values computed for individual 30-min averaged points. Note that our plots in Fig. 10 are consistent with the results of Horst and Doran (1988, their Figs. 2, 3) and Smeets et al. (2000, their Fig. 10). Although the data presented in Fig. 10 generally prove the validity of the z-less approach (13), the plots in Fig. 10 are affected by self-correlation because u_* appears both in the definitions of the universal functions φ_α and in ζ. This results in a weak trend of the data points in Fig. 10. However, this flaw can be overcome by plotting φ_α versus a stability parameter that does not contain u_* (see Grachev et al. 2013, 2015 for discussion).

Figure 11 shows plots of the non-dimensional universal functions φ_m, Eq. 8 and φ_ε, Eq. 9, versus the Monin–Obukhov stability parameter for local scaling $\zeta = n/L \approx z/L$, Eq. 3. According to Fig. 11 our data are consistent with the linear interpolations $\varphi_m(\zeta) = 1 + \beta_m \zeta$ and $\varphi_\varepsilon(\zeta) = 1 + \beta_\varepsilon \zeta$ with numerical coefficients $\beta_m = 4.1$ (Fig. 11a) and $\beta_\varepsilon = 5.2$ (Fig. 11b), and, therefore, the data are consistent with the z-less predictions (11) and (12).

Similarly to plots shown in Figs. 3, 4, 5, 6 and 7, the turbulent fluxes and variances in Figs. 10 and 11 are computed through frequency integration over the high-frequency portions of the appropriate spectra and cospectra. Because here we only consider a region above the slope jet, data collected at levels 3–7 of the ES2 tower, levels 3–5 of the ES3 and ES5 towers, and levels 4–6 of the ES4 tower are only analyzed in Figs. 10 and 11. All six cases of westerly katabatic flow mentioned in Sect. 4 are used in Figs. 10 and 11 (records were only accepted if the true wind direction at all towers and all levels was within a 280 ± 30° sector).

Furthermore, the data presented in Figs. 10 and 11 were quality controlled prior to evaluating similarity functions (8)–(10) in order to remove spurious or low-quality records. The

Journal: 10546-BOUN Article No.: 0034 TYPESET DISK LE CP Disp.:2015/5/2 Pages: 26 Layout: Small

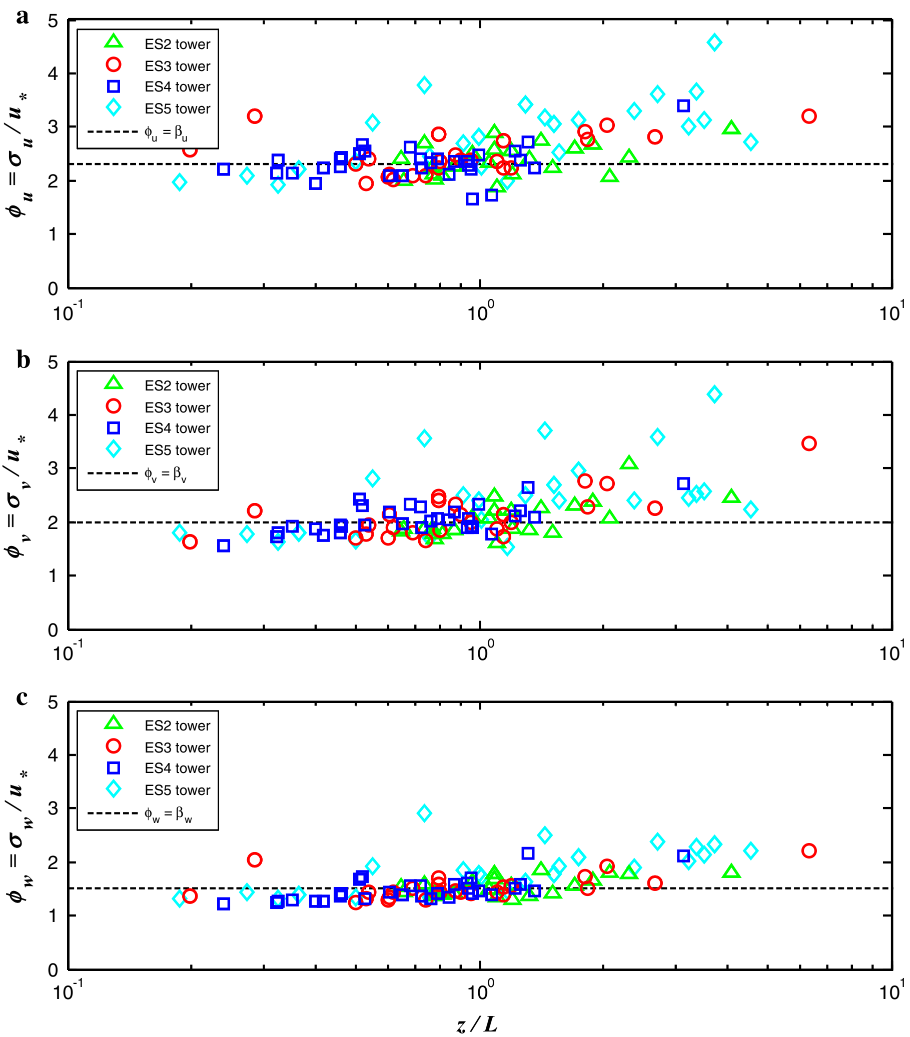

Fig. 10 The non-dimensional standard deviations of **a** longitudinal (down-slope), **b** lateral (cross-slope), and **c** vertical (normal) wind speed component (local scaling) observed for katabatic winds in the layer above the slope jet at the ES2–ES5 flux towers on the east slope of Granite Mountain. The *horizontal dashed lines* correspond to $\beta_u = 2.3$, $\beta_v = 2.0$, and $\beta_w = 1.5$

following filtering criteria are adopted (see Grachev et al. 2013, 2015 and references therein for discussion): to avoid a possible flux loss caused by inadequate frequency response and sensor separations, we omitted data with a local wind speed less than 0.2 m s^{-1}. We set minimum and/or maximum thresholds for the kinematic momentum flux (>0.0002 m^2 s^{-2}), vertical and along-slope temperature fluxes (<–0.0002 K m s^{-1}), standard deviation of each wind-speed component (>0.01 m s^{-1}), standard deviation of air temperature (>0.01 K), vertical gradients of mean wind speed (<–0.001 s^{-1}), dissipation rate of TKE ($0.00002 < \varepsilon < 0.1$ m^2 s^{-3}) and the dissipation (destruction) rate for half the temperature variance ($0.00002 < N_t < 0.01$ K^2 s^{-1}). Points with excessive standard deviations of wind direction (>30°), steadiness

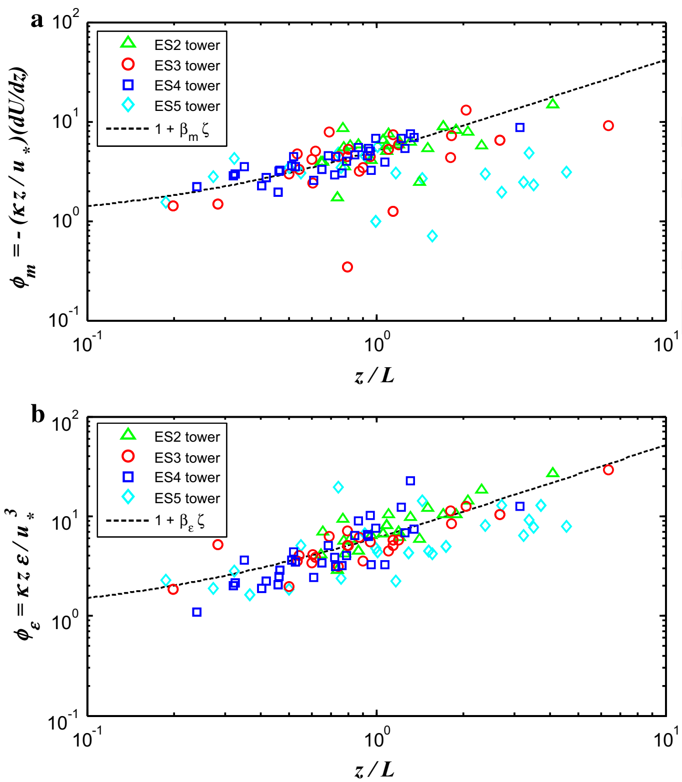

Fig. 11 Same as Fig. 10 but for the non-dimensional universal functions **a** φ_m and **b** φ_ε. The *dashed lines* are based on $\beta_m = 4.1$ and $\beta_\varepsilon = 5.1$. Note that the function φ_m is defined as positive for negative vertical gradients of mean wind speed in the layer above a wind-speed maximum

(trend) of the non-rotated wind-speed components ($\Delta u/U < 1$, $\Delta v/U < 1$), and sonic temperature (>2 °C) were also removed to avoid non-stationary conditions during a 30-min record. In addition, sonic anemometer angles of attack were limited to 10°.

5 Summary and Conclusions

We described and discussed the small-scale turbulence structure of katabatic flows based on tower measurements made over complex terrain during the first MATERHORN field campaign (MATERHORN–Fall) at the US Army Dugway Proving Grounds in Utah from 25 September through 31 October 2012. Turbulent and mean meteorological data were collected at multiple levels (up to seven) on four ES2–ES5 flux towers deployed along the east slope (2–4°) of Granite Mountain (Figs. 1, 2), allowing for study of the temporal and spatial structure of nocturnal slope flows in detail, and providing insights into the nature of the phenomenon.

Katabatic flows develop soon after sunset when the surface starts to cool, and are associated with quiescent synoptic conditions and clear skies. In general, these flows are considered to be unidirectional and persistent. It is found, however, that westerly katabatic flows over the east slope of Granite Mountain are rather intermittent due to interactions with valley flows

Journal: 10546-BOUN Article No.: 0034 TYPESET DISK LE CP Disp.:2015/5/2 Pages: 26 Layout: Small

occurring at various times during the night. In general, the flow appears to be free from such interactions soon after sunset, for a duration of about 2–3 h. In our study we analyzed only such flows that resemble a "pure" katabatic flow structure at all ES2–ES4 flux towers at the same time.

The most prominent feature of katabatic flows is a wind-speed maximum close to the surface (Figs. 3a, 5a, 6a) that causes a change in sign of the vertical momentum flux (downslope stress), $\tau = -\langle u'w' \rangle$, and the along-slope temperature (density) flux, $\langle u'\theta_v' \rangle$ below and above this maximum. According to our data, $\langle u'w' \rangle$ is negative (positive) whereas $\langle u'\theta' \rangle$ is positive (negative) below (above) the wind-speed maximum (Figs. 3c, 5b, 6b and Figs. 4a, 6d respectively). In other words, the vertical momentum flux is downward (upward) whereas the along-slope temperature flux is downslope (upslope) below (above) the wind-speed maximum in a slope-following coordinate system. We suggest that the position of the jet-speed maximum can be derived from linear interpolation between positive and negative values of the momentum flux (or the along-slope heat flux) and determination of the height where the flux becomes zero. Furthermore, it is shown that the standard deviations of all wind-speed components (and therefore TKE) and the dissipation rate of TKE have a local minimum (Fig. 4c, d), whereas the standard deviation of air temperature σ_t has an absolute maximum (Figs. 4b, 5c) near a wind-speed maximum.

It is found that the profiles of velocity, turbulent fluxes, and other quantities have steep gradients in the layer below a wind-speed maximum (Figs. 3, 4, 5, 6). Above the slope jet, however, the wind speed, temperature, turbulent fluxes, and variances vary with height more slowly than near the surface (approximately an order of magnitude). According to our data (Figs. 3, 4, 5), the vertical profiles of wind speed, turbulent fluxes, and variances are approximately stationary in time (especially near the surface) for a given tower during specific time intervals. However, the vertical profiles of wind speed and turbulent fluxes along the tower line vary widely for a given time period, characterizing the spatial evolution of the flow (Fig. 6).

Slope flows are traditionally described and modelled in a slope-following coordinate system. Because the mean flow is not normal to the direction of gravity, the buoyancy term in the turbulence equations include extra terms associated with the along-slope heat flux, $\beta \langle u'\theta_v' \rangle \sin\alpha$, which can enhance or suppress turbulence. The along-slope heat flux is a sink (source) for TKE below (above) the wind maximum, and, therefore, in slope flows R_f and z/L below (above) the wind maximum are smaller (larger) than over flat horizontal surfaces. Moreover, we describe several cases when $\langle u'\theta_v' \rangle / \langle w'\theta_v' \rangle \approx 19$ (Fig. 7a, b), implying that the net buoyancy term $\beta \left(\langle w'\theta_v' \rangle \cos\alpha - \langle u'\theta_v' \rangle \sin\alpha \right) \approx 0$ for typical slopes at the east slope site ($\alpha \approx 2{-}4°$). In this case the destructive effect of vertical heat (buoyancy) flux is completely cancelled by the generation of turbulence due to the along-slope heat (buoyancy) flux.

The zero wind shear, change in the sign of momentum flux, local minimum in TKE and dissipation rate, and the background stable stratification suggest that turbulence in the layer above the wind-speed maximum is decoupled from the surface. In other words, turbulence no longer communicates significantly with the surface, making the height of the measurement z irrelevant as a governing parameter. We hypothesize that turbulence in this layer is consistent with the classical local z-less (height-independent) predictions for the stably stratified boundary layer. The normalized standard deviations of all three wind-speed components, the non-dimensional vertical gradient of mean wind speed, and the non-dimensional dissipation rate of turbulent kinetic energy were in good agreement with the z-less concept (Figs. 10, 11).

Journal: 10546-BOUN Article No.: 0034 TYPESET DISK LE CP Disp.:2015/5/2 Pages: 26 Layout: Small

Acknowledgments The MATERHORN Program was funded by the Office of Naval Research with award # N00014-11-1-0709, with additional funding from the Army Research Office, Air Force Weather Agency, University of Notre Dame, and University of Utah. Special thanks go to Evgeni Fedorovich who pointed out the importance of the horizontal (along-slope) heat flux in the net buoyancy term in the TKE equation and in the modified Monin–Obukhov stability parameter. We also appreciate useful comments and suggestions from three anonymous reviewers.

References

Axelsen SL, van Dop H (2009a) Large-eddy simulation of katabatic winds. Part 1: comparison with observations. Acta Geophys 57(4):803–836. doi:10.2478/s11600-009-0041-6

Axelsen SL, van Dop H (2009b) Large-eddy simulation of katabatic winds. Part 2: sensitivity study and comparison with analytical models. Acta Geophys 57(4):837–856. doi:10.2478/s11600-009-0042-5

Axelsen SL, Shapiro A, Fedorovich E, van Dop H (2010) Analytical solution for katabatic flow induced by an isolated cold strip. Environ Fluid Mech 10(4):387–414. doi:10.1007/s10652-009-9158-z

Banta RM, Pichugina YL, Brewer WA (2006) Turbulent velocity-variance profiles in the stable boundary layer generated by a nocturnal low-level jet. J Atmos Sci 63(11):2700–2719

Brooks IM, Söderberg S, Tjernström M (2003) The turbulence structure of the stable atmospheric boundary layer around a coastal headland: aircraft observations and modeling results. Boundary-Layer Meteorol 107(3):531–559. doi:10.1023/A:1022822306571

Clements WE, Archuleta JA, Hoard DE (1989) Mean structure of the nocturnal drainage flow in a deep valley. J Appl Meteorol 28(6):457–462

Denby B (1999) Second-order modelling of turbulence in katabatic flows. Boundary-Layer Meteorol 92(1):67–100. doi:10.1023/A:1001796906927

Denby B, Smeets CJPP (2000) Derivation of turbulent flux profiles and roughness lengths from katabatic flow dynamics. J Appl Meteorol 39(9):1601–1612

Egger J (1990) Thermally forced flows: theory. In: Blumen W (ed) Atmospheric processes over complex terrain. American Meteorological Society, Washington DC, pp 43–57 (323 pp)

Fedorovich E, Shapiro A (2009) Structure of numerically simulated katabatic and anabatic flows along steep slopes. Acta Geophys 57(4):981–1010. doi:10.2478/s11600-009-0027-4

Fernando HJS, Pardyjak ER, Di Sabatino S, Chow FK, De Wekker SFJ, Hoch SW, Hacker J, Pace JC, Pratt T, Pu Z, Steenburgh JW, Whiteman CD, Wang Y, Zajic D, Balsley B, Dimitrova R, Emmitt GD, Higgins CW, Hunt JCR, Knievel JC, Lawrence D, Liu Y, Nadeau DF, Kit E, Blomquist BW, Conry P, Coppersmith RS, Creegan E, Felton M, Grachev A, Gunawardena N, Hang C, Hocut CM, Huynh G, Jeglum ME, Jensen D, Kulandaivelu V, Lehner M, Leo LS, Liberzon D, Massey JD, McEnerney K, Pal S, Price T, Sghiatti M, Silver Z, Thompson M, Zhang H, Zsedrovits T (2015) The MATERHORN - unraveling the intricacies of mountain weather. Bull Amer Meteor Society, In press

Geissbuhler P, Siegwolf R, Eugster W (2000) Eddy covariance measurements on mountain slopes: the advantage of surface-normal sensor orientation over a vertical set-up. Boundary-Layer Meteorol 96(3):371–392. doi:10.1023/A:1002660521017

Grachev AA, Fairall CW (2001) Upward momentum transfer in the marine boundary layer. J Phys Oceanogr 31(7):1698–1711

Grachev AA, Andreas EL, Fairall CW, Guest PS, Persson POG (2013) The critical Richardson number and limits of applicability of local similarity theory in the stable boundary layer. Boundary-Layer Meteorol 147(1):51–82. doi:10.1007/s10546-012-9771-0

Grachev AA, Andreas EL, Fairall CW, Guest PS, Persson POG (2015) Similarity theory based on the Dougherty-Ozmidov length scale. Q J R Meteorol Soc. doi:10.1002/qj.2488

Grisogono B (2003) Post-onset behaviour of the pure katabatic flow. Boundary-Layer Meteorol 107:157–175

Grisogono B, Axelsen SL (2012) A note on the pure katabatic wind maximum over gentle slopes. Boundary-Layer Meteorol 145(3):527–538

Grisogono B, Oerlemans J (2001a) Katabatic flow: analytic solution for gradually varying eddy diffusivities. J Atmos Sci 58(21):3349–3354

Grisogono B, Oerlemans J (2001b) A theory for the estimation of surface fluxes in simple katabatic flows. Q J R Meteorol Soc 127(578B):2725–2739

Grisogono B, Zovko Rajak D (2009) Assessment of Monin–Obukhov scaling over small slopes. Geofizika 26(1):101–108

Haiden T, Whiteman CD (2005) Katabatic flow mechanisms on a low-angle slope. J Appl Meteorol 44(1):113–126

Hanley KE, Belcher SE (2008) Wave-driven wind jets in the marine atmospheric boundary layer. J Atmos Sci 65(8):2646–2660

Harris DL (1966) The wave-driven wind. J Atmos Sci 23(6):688–693

Hartogensis OK, De Bruin HAR (2005) Monin–Obukhov similarity functions of the structure parameter of temperature and turbulent kinetic energy dissipation rate in the stable boundary layer. Boundary-Layer Meteorol 116(2):253–276. doi:10.1007/s10546-004-2817-1

Helmis CG, Papadopoulos KH (1996) Some aspects of the variation with time of katabatic flow over a simple slope. Q J R Meteorol Soc 122(531A):595–610. doi:10.1002/qj.49712253103

Hocut CM, Hoch SW, Fernando HJS, Leo LS, Di Sabatino S, Wang Y, Pardyjak ER, Whiteman CD (2015) Interactions between slope and valley flows. J Atmos Sci (in preparation)

Horst TW, Doran JC (1986) Nocturnal drainage flow on simple slopes. Boundary-Layer Meteorol 34(3):263–286

Horst TW, Doran JC (1988) The turbulence structure of nocturnal slope flow. J Atmos Sci 45(4):605–616

Ingel' LKh (2000) Nonlinear theory of slope flows. Russian Acad Sci Atmos Oceanic Phys (Izvestiya) 36:384–389

Kaimal JC, Finnigan JJ (1994) Atmospheric Boundary Layer Flows: Their Structure and Measurements. Oxford University Press, New York 289 pp

Kavčič I, Grisogono B (2007) Katabatic flow with Coriolis effect and gradually varying eddy diffusivity. Boundary-Layer Meteorol 125(2):377–387. doi:10.1007/s10546-007-9167-8

Kochendorfer J, Meyers TP, Frank J, Massman WJ, Heuer MW (2012) How well can we measure the vertical wind speed? Implications for fluxes of energy and mass. Boundary-Layer Meteorol 145(2):383–398. doi:10.1007/s10546-012-9738-1

Kouznetsov R, Tisler P, Palo T, Vihma T (2013) Evidence of very shallow summertime katabatic flows in Dronning Maud Land, Antarctica. J Appl Meteorol Climatol 52(1):164–168

Łobocki L (2014) Surface-layer flux–gradient relationships over inclined terrain derived from a local equilibrium, turbulence closure model. Boundary-Layer Meteorol 150(3):469–483. doi:10.1007/s10546-013-9888-9

Lykosov VN, Gutman LN (1972) Turbulent boundary layer above a sloping underlying surface. Izvestiya. Acad Sci USS. Atmos Oceanic Phys 8:799–809

Mahrt L (1982) Momentum balance of gravity flows. J Atmos Sci 39(12):2701–2711

Manins PC, Sawford BL (1979) Katabatic winds: A field case study. Q J R Meteorol Soc 105(446):1011–1025. doi:10.1002/qj.49710544618

Mauder MA (2013) A comment on "How well can we measure the vertical wind speed? Implications for fluxes of energy and mass" By Kochendorfer, et al. Boundary-Layer Meteorol 147(2):329–335. doi:10.1007/s10546-012-9794-6

Meesters AGCA, Bink NJ, Henneken EAC, Vugts HF, Cannemeijer F (1997) Katabatic wind profiles over the Greenland ice sheet: observation and modelling. Boundary-Layer Meteorol 85(3):475–496. doi:10.1023/A:1000514214823

Monti P, Fernando HJS, Princevac M, Chan WC, Kowalewski TA, Pardyjak ER (2002) Observations of flow and turbulence in the nocturnal boundary layer over a slope. J Atmos Sci 59(17):2513–2534

Monti P, Fernando HJS, Princevac M (2014) Waves and turbulence in katabatic winds. Environ Fluid Mech 14(2):431–450. doi:10.1007/s10652-014-9348-1

Nadeau DF, Pardyjak ER, Higgins CW, Huwald H, Parlange MB (2013a) Flow during the evening transition over steep Alpine slopes. Q J R Meteorol Soc 139(672A):607–624. doi:10.1002/qj.1985

Nadeau DF, Pardyjak ER, Higgins CW, Parlange MB (2013b) Similarity scaling over a steep alpine slope. Boundary-Layer Meteorol 147(3):401–419. doi:10.1007/s10546-012-9787-5

Neff WD (1990) Remote sensing of atmospheric processes over complex terrain. In: Blumen W (ed) Atmospheric processes over complex terrain. Meteorological Monographs, vol 23, No. 45. American Meteorology Society, Boston, MA, pp 173–228

Neff WD, King CW (1987) Observations of complex terrain flows using acoustic sounders: experiments, topography and winds. Boundary-Layer Meteorol 40(4):363–392. doi:10.1007/BF00116103

Neff WD, King CW (1988) Observations of complex terrain flows using acoustic sounders: drainage flow structure and evolution. Boundary-Layer Meteorol 43(1–2):15–41. doi:10.1007/BF00153967

Oerlemans J, Grisogono B (2002) Glacier wind and parameterisation of the related surface heat flux. Tellus 54:440–452

Oerlemans J, Björnsson H, Kuhn M, Obleitner F, Palsson F, Smeets CJPP, Vugts HF, de Wolde J (1999) Glacio-meteorological investigations on Vatnajökull, Iceland, summer 1996: an overview. Boundary-Layer Meteorol 92(1):3–26. doi:10.1023/A:1001856114941

Oldroyd HJ, Katul G, Pardyjak ER, Parlange MB (2014) Momentum balance of katabatic flow on steep slopes covered with short vegetation. Geophys Res Lett 41: doi:10.1002/2014GL060313

Journal: 10546-BOUN Article No.: 0034 TYPESET DISK LE CP Disp.:2015/5/2 Pages: 26 Layout: Small

Papadopoulos KH, Helmis CG, Soilemes AT, Kalogiros J, Papageorgas PG, Asimakopoulos DN (1997) The structure of katabatic flows down a simple slope. Q J R Meteorol Soc 123(542B):581–1601. doi:10.1002/qj.49712354207

Pardyjak ER, Fernando HJS, Hunt JCR, Grachev AA, Anderson JA (2009) A case study of the development of nocturnal slope flows in a wide open valley and associated air quality implications. Meteorologische Zeitschrift 18(1):85–100

Parmhed O, Oerlemans J, Grisogono B (2004) Describing surface-fluxes in katabatic flow on Breidamerkurjökull, Iceland. Q J R Meteorol Soc 130(598):1137–1151

Pichugina YL, Banta RM (2010) Stable boundary layer depth from high-resolution measurements of the mean wind profile. J Appl Meteorol Climatol 49(1):20–35

Poulos G, Zhong S (2008) An observational history of small-scale katabatic winds in mid-latitudes. Geogr Compass 2(6):1798–1821. doi:10.1111/j.1749-8198.2008.00166.x

Prandtl L (1942) Führer durch die Strömungslehre. Vieweg und Sohn, Braunschweig 382 pp

Princevac M, Fernando HJS, Whiteman CD (2005) Turbulent entrainment into nocturnal gravity-driven flow. J Fluid Mech 533:259–268

Princevac M, Hunt JCR, Fernando HJS (2008) Quasi-steady katabatic winds on slopes in wide valleys: hydraulic theory and observations. J Atmos Sci 65(2):627–643

Renfrew IA (2004) The dynamics of idealized katabatic flow over a moderate slope and ice shelf. Q J R Meteorol Soc 130(598):1023–1045. doi:10.1256/qj.03.24

Renfrew IA, Anderson PS (2006) Profiles of katabatic flow in summer and winter over Coats Land, Antarctica. Q J R Meteorol Soc 132(616A):779–802. doi:10.1256/qj.05.148

Shapiro A, Fedorovich E (2008) Coriolis effects in homogeneous and inhomogeneous katabatic flows. Q J R Meteorol Soc 134(631):353–370. doi:10.1002/qj.217

Shapiro A, Fedorovich E (2014) A boundary-layer scaling for turbulent katabatic flow. Boundary-Layer Meteorol 153(1):1–17. doi:10.1007/s10546-014-9933-3

Skyllingstad ED (2003) Large-eddy simulation of katabatic flows. Boundary-Layer Meteorol 106(2):217–243. doi:10.1023/A:1021142828676

Smedman A-S, Tjernström M, Högström U (1994) Near-neutral marine atmospheric boundary layer with no surface shearing stress: a case study. J Atmos Sci 51(23):3399–3411

Smeets CJPP, Duynkerke PG, Vugts HF (1998) Turbulence characteristics of the stable boundary layer over a mid-latitude glacier. Part I: a combination of katabatic and large-scale forcing. Boundary-Layer Meteorol 87(1):117–145. doi:10.1023/A:1000860406093

Smeets CJPP, Duynkerke PG, Vugts HF (2000) Turbulence characteristics of the stable boundary layer over a mid-latitude glacier. Part II: pure katabatic forcing conditions. Boundary-Layer Meteorol 97(1):73–107. doi:10.1023/A:1002738407295

Smith CM, Porté-Agel F (2013) An intercomparison of subgrid models for large-eddy simulation of katabatic flows. Q J R Meteorol Soc. doi:10.1002/qj.2212

Smith CM, Skyllingstad ED (2005) Numerical simulation of katabatic flow with changing slope angle. Mon Weather Rev 133:3065–3080

Söderberg S, Parmhed O (2006) Numerical modelling of katabatic flow over a melting outflow glacier. Boundary-Layer Meteorol 120(3):509–534. doi:10.1007/s10546-006-9059-3

Söderberg S, Tjernström M (2004) Modeling the turbulent structure of the katabatic jet. In: 16th Symposium on boundary layers and turbulence, Portland, ME, 9–13 August 2004. American Meteorological Society, 4 pp. https://ams.confex.com/ams/BLTAIRSE/techprogram/paper_78149.htm

Stiperski I, Kavčič I, Grisogono B, Durran DR (2007) Including Coriolis effects in the Prandtl model for katabatic flow. Q J R Meteorol Soc 133:101–106

Stone GL, Hoard DE (1989) Low-frequency velocity and temperature fluctuations in katabatic valley flows. J Appl Meteorol 28(6):477–488

Tse KL, Mahalov A, Nicolaenko B, Fernando HJS (2003) Quasi-equilibrium dynamics of shear-stratified turbulence in a model tropospheric jet. J Fluid Mech 496:73–103. doi:10.1017/S0022112003006487

Van den Broeke M (1997) Momentum, heat, and moisture budgets of the katabatic wind layer over a midlatitude glacier in summer. J Appl Meteorol 36(6):763–774

Van der Avoird E, Duynkerke PG (1999) Turbulence in a katabatic flow. Does it resemble turbulence in a stable boundary layer over flat surfaces? Boundary-Layer Meteorol 92(1):39–66. doi:10.1023/A:1001744822857

Van Gorsel E, Christen A, Feigenwinter C, Parlow E, Vogt R (2003) Daytime turbulence statistics above a steep forested slope. Boundary-Layer Meteorol 109(3):311–329. doi:10.1023/A:1025811010239

Viana S, Terradellas E, Yagüe C (2010) Analysis of gravity waves generated at the top of a drainage flow. J Atmos Sci 67(12):3949–3966

Journal: 10546-BOUN Article No.: 0034 TYPESET DISK LE CP Disp.:2015/5/2 Pages: 26 Layout: Small

Whiteman CD (2000) Mountain meteorology: fundamentals and applications. Oxford University Press, New York 376 pp

Whiteman CD, Zhong S (2008) downslope flows on a low-angle slope and their interactions with valley inversions. Part I: observations. J Appl Meteorol Climatol 47(7):2023–2038

Wyngaard JC, Coté OR (1972) Cospectral similarity in the atmospheric surface layer. Q J R Meteorol Soc 98:590–603

Zammett RJ, Fowler AC (2007) Katabatic winds on ice sheets: a refinement of the Prandtl model. J Atmos Sci 64(7):2707–2716